SORPTION AND DIFFUSION OF ETHYL ACETATE VAPOR IN POLYIMIDE-CLAY NANOCOMPOSITE FILMS

By

Wenzhen Cheng

A THESIS

Submitted to

Michigan State University

In partial fulfillment of the requirements

for the degree of

MASTER OF SCIENCE

School of Packaging

1999

ABSTRACT

SORPTION AND DIFFUSION OF ETHYL ACETATE VAPOR IN POLYIMIDE-CLAY NANOCOMPOSITE FILMS

By
Wenzhen Cheng

Sorption and diffusion of an organic vapor are key processes to gain an understanding of the mass transfer properties of polyimide-clay nanocomposite films. The sorption characteristics of ethyl acetate vapor in polyimide-clay films were determined by micro-gravimetry and the diffusion characteristics were calculated from the sorption kinetics at different vapor activities, by curve fitting. The vapor activity dependence of the solubility and diffusion coefficients, S and D, respectively, is represented by a modified dual-mode sorption model and a tortuosity model. The montmorillonite clay mineral, which is hybridized with a polyimide, consists of stacked silicate sheets about 10 Å in thickness, and 800 ~ 2000 Å in length. In this nanocomposite film, montmorillonite is dispersed homogeneously into the polyimide matrix and oriented parallel to the film surface. Due to this structure, the nanocomposite showed excellent organic vapor barrier properties. Only a small volume fraction of clay (i.e. 2.5v/v%) resulted in a significant decrease in the diffusion coefficient. Furthermore, solubility and solubility coefficient values for the polyimide-clay composites were similar to those obtained for the non-clay loading polyimide films, over the range of ethyl acetate vapor activity levels studied. The permeant studies indicated that the organic vapor diffusion coefficients increased exponentially with an increase in local penetrant concentration within the polymer membrane. The studied also showed that the diffusion coefficients decreased dramatically with an increase in clay loading level of the polymer membranes.

To

My beautiful wife, Xiaole

&

Lovely baby boy, Christopher

Acknowledgements

Thank god for giving me a precious opportunity to study and to have a good time in School of Packaging of Michigan State University.

I would like to thank Dr. Jack Giacin from my heart. During the years of study, Dr. Giacin has given me a generous financial support and valuable academic advice. Without this, I can't complete my study and this project. Also, I would like to thank my co-advisor Dr. Ruben Hernandez and Dr. Thomas Pinnavaia, for their sourceful guidance through the entire project. I appreciate Christopher Barr, former graduated student, for helping me get started with this research project. In addition, I am very grateful to the Center for Fundamental Materials Research whose funding made this project possible.

Finally, my wife and my son deserve my deepest love for their love, support and good will during the years studying in this far-away-from-home country.

Table of Contents

List of Tables

List of Figures

List of Symbols and Abbreviations

a_v	penetrant activity
ℓ	Film thickness, m
φ	represents F_t/F_∞
b	hole affinity constant, pa^{-1}
C_{exp}	experimental solubility values, g/g sorbant
C_{est}	calculated solubility values, g/g sorbant
C_p	solubility values of polyimide matrix, g/g sorbant
C_c	solubility values of clay powder, g/g sorbant
c	concentration of the standard solution for gas chromatography analysis, cc/cc
C_A	vapor concentration of point A, cc gas(STP)/cc polymer
C_B	vapor concentration of point B, cc gas(STP)/cc polymer
C'_H	hole saturation constant, cc[STP]/cc polymer
D	concentration independence diffusion coefficient, m^2/sec
D*	limiting diffusion coefficient, m^2/sec
d	thickness of a film, m
d'	total path of a diffusing gas, m
D_c	diffusion coefficient of nanocomposite, m^2 / sec
D_p	diffusion coefficient of polymer matrix, m^2 / sec
F_∞	permeation rate of permeation flux after infinite time
F_A	gas flow rate at point A, cc/sec
F_B	gas flow rate at point B, cc/sec

F_t	permeation rate of permeation flux at time t
J	rate of diffusion
k_D	Henry's law constant, cc[STP]/cc · pa^{-1}
L	length of the clay platelet, m
M_∞ (or M_{ss})	total amount of the sorbate uptake in the polymer after infinite time, g
$M_{calc.}$	theoretical amount of the sorbate uptake in the polymer at time t, g
$M_{exp.}$	experimental data of the sorbate uptake in the polymer at time t, g
M_t	total amount of the sorbate uptake in the polymer at time t, g
P	steady state permeability coefficient, cc[STP] · m/m^2 · pa · sec
p	vapor partial pressure, *pa*
p_A	vapor partial pressure at point A, *pa*
p_B	vapor partial pressure at point B, *pa*
P_c	permeability coefficient of nanocomposite, cc[STP] · m/m^2 · pa · sec
p_i	test vapor partial pressure of ethyl acetate, pa
τ	tortuosity factor
γ	a coefficient of Equation 43
P_p	permeability coefficient of polymer matrix, cc[STP] · m/m^2 · pa · sec
p_s	saturation vapor pressure of ethyl acetate, pa
q_i	quantity injected for gas chromatography analysis, g
S	solubility coefficient, cc[STP]/cc · pa^{-1}
S_c	solubility coefficient of nanocomposite, m^2 / sec
S_p	solubility coefficient of polymer matrix, m^2 / sec
t	time of sorption experimental, sec

T_A	Temperature of point A, °C
T_B	Temperature of point B, °C
V_A	volume of the system at point A, cc
V_B	volume of the system at point B, cc
v_f	volume fraction of a clay
W	width of the clay platelet, m
X	represents $\ell^2/4D\,t$

Introduction

The sorption and diffusion of low molecular weight compounds, such as water vapor and organic vapors, are of major concern in the use and application of polymeric packaging materials, since such product/package systems are typically stored in an environment which may contain organic and/or water vapors. New packaging materials with high strength, light weight, high barrier, more functionality and low cost are expected to be developed for future industry use.

For the purpose of these applications, polyimides have been evaluated as a promising class of material, with potential applications in packaging. Polyimides are widely used for microelectronics because they exhibit high heat resistance, chemical stability and superior electric properties (Ghosh, 1996). In recent years, composite films made of polyimide have been used as membranes for the industrial dehydration of organic vapor by the per-vaporization membrane process (Okamoto et al., 1992). Polyimide membranes may also have packaging applications, such as in electronic packaging, where the barrier property of the package system is one of the major concerns. It would be desirable to reduce the cost and amount of vapor absorption by polyimides, as well as to enhance their barrier properties, since those properties of polyimides are not sufficient for advanced electronics use.

Polymer-clay nanocomposites are a new class of material designed to meet these demands. In this case, the nano-size clay layers (10 Å - thick) are homogeneously dispersed in the polymer matrix. Due to their specific molecular composition, nanocomposites usually exhibit significant enhancement in mechanical, optical, conductive, nonlinear optical and barrier properties, as compared to the single components and conventional composites (Lan, 1994).

.

As montmorillonite is composed of stacked silicate sheets, it has a low thermal expansion coefficient and high gas barrier properties (Yano et al., 1993). Polymer-clay nanocomposites are usually stable after the hybrid complexes are formed, and do not undergo phase separation. The synthesis and properties of a polyimide-clay nanocomposite had been reported in the early 90's by Yano (1991). It was found that when a specific ammonium ion is chosen as the intercalating reagent, montmorillonite disperses homogeneously in dimethyl-acetamide, which is a solvent for the preparation of polyimides. The montmorillonite dispersion can be mixed with the precursor solution of the polyimide, and after removing the solvent, the polyimide-clay nanocomposite membranes were obtained. The resultant polyimide-clay nanocomposite showed excellent gas barrier properties to CO_2, O_2 and water vapor. Organic vapor permeability of the nanocomposite membranes has also been reported for 2.5 % (v/v) polyimide-clay nanocomposite film and showed an 85% reduction in organic vapor transmission rate, when compared to the polyimide film without clay inclusion (Gu, 1997).

The solubility and diffusivity of a penetrant in a polymer membrane depends on the temperature and the vapor activity in contact with the polymer. Knowledge of the correlation between the solubility and diffusion coefficients of the penetrant in the polymer membrane and penetrant vapor activity in the atmosphere surrounding the membrane, would make possible the calculation of either the variation of penetrant sorption extent with time on the specific conditions, or its permeability rate through the membrane. Yano (1993) reported that the diffusion coefficient of O_2 and water vapor in polyimide/clay hybrid could be well explained by the tortuosity model. In the present study, the sorption and diffusion characteristics of ethyl acetate vapor in polyimide were described by microgravimetry and the tortuosity model.

The objective of the study is to gain an understanding of the mass transfer properties of nanocomposites derived from organic polymers and plate-like inorganic inclusions (i.e. clays) and organic penetrants, and the principles governing the barrier properties of nanocomposites derived from organic polymers and plate-like inorganic inclusions.

The present study therefore includes measurements of the sorption and diffusion of ethyl acetate into polyimide membranes with and without clay inclusion, over a range of sorbate activities. Isotherms were determined gravimetrically at 23 ± 1 °C, 0% RH at 0, 1.25, 2.5 and 5 % (v/v) clay loading. To provide insight into the activity dependence of the mass transfer process, seven vapor activity levels were evaluated: 0.15, 0.21, 0.27, 0.34, 0.44, 0.55 and 0.68, respectively.

Literature Review

Polymer-Clay Nanocomposite

1. General Concepts of Nanocomposites

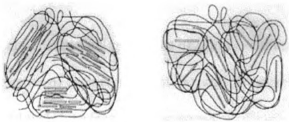

Figure 1. Structure differences between intercalated and exfoliated polymer-clay nanocomposites.

In general, there are two categories of polymer-clay nanocomposites, as presented above in Figure 1. As shown, the intercalated and exfoliated nanocomposites exhibit structural differences. Compared to the nanocomposite, the clay tactoids in conventional composites exist in their original aggregated state with no intercalation of the polymer matrix into the clay gallery regions. The intercalated polymer-clay nanocomposites are of interest because organic polymer layers and inorganic silicate layers are alternatively interstratified at the molecular level --- at least one dimension in the size range ot a nanometer (1×10^{-9} meter, or $1/25 \times 10^{-6}$ inch) (Nanocor, Inc. web page, 1997).

Polymer/clay nanocomposites are differentiated from conventional composites by the fact that the size of the fillers is so small that the nanocomposite is macroscopically homogenous. Exfoliated polymer-clay nanocomposites possess unique structural and mechanical properties. For example, the exfoliated clay layers (10 Å - thick), which are dispersed into the polymer matrix, simulate the fibers in fiber-reinforced-plastics (Lan, 1994).

The physical and mechanical properties of a nanocomposite are determined not only by the bulk properties of each component, but also by complex interactions between the building blocks and their interface. Nanocomposites usually exhibit a significant enhancement in mechanical, optical, conductive, nonlinear optical and barrier properties, over the individual components and conventional composites containing simple fillers (Pinnavaia, 1997).

2. Recent Studies and Advances in Polymer-clay Nanocomposites

Polymer-clay composites have been studied since 1965 (Blumstein, 1965) (Lagaly and Beneke, 1975). It was not until Toyota researchers developed several nanoscale polymer-clay hybrid composites, however, that polymer-clay nanocomposites have become the subject of significant research efforts (Fukushima and Inagaki, 1987). These studies were based on the dispersion of an ω-amino acid and alkylammonium exchanged forms of montomorilonite clay into:

i) semicrystalline nylon-6 (Fukushima and Inagaki, 1987), (Usuki et al., 1995)

ii) amorphous epoxy (Usuki et al., 1989),

iii) acrylic resin (Usuki et al., 1995(a)),

iv) polyimide (Yano et al., 1993), (Lan and Pinnavaia, 1994(a)).

At present, there are three major research groups working on polymer-clay nanocomposites. These include Giannelis's group at Cornell University, the Toyota group at Toyota Central R&D lab, Inc. Japan, and Pinnavaia's group at Michigan State University.

Two different synthetic methods are commonly used to prepare intercalated clay polymer nanocomposites. One procedure involves preformed-polymer-intercalation, where the preformed polymer and clays, respectively, are dissolved and dispersed in a compatible solvent, and then mixed. Water-soluble polymers can be intercalated into

clay galleries by this method. Such systems include (i) polyethylene oxide (Ruiz-Hitzky, 1993); (ii) ethylene-vinyl alcohol copolymer (Tohoh, 1992); and (iii) polyvinyl alcohol (Greenland, 1963). Molten polymers can also be intercalated in this way. For example, polystyrene was intercalated into organo-montmorillonite clays (Vaia et al., 1993). The second method is the "*in situ*" intercalative polymerization procedure. In this procedure, the desired monomers are adsorbed or intercalated into the clay galleries. The intercalated monomers are then polymerized within the clay galleries to form the polymer-clay nanocomposite. This method has been used extensively to modify a number of engineering polymers to include: polyamide (Kato et al., 1979), polymethyl metharcylate (Blumstein, 1965), polyimide (Yano et al., 1993), polyaniline (Mehrotra and Giannelis, 1990), poly(ε-caprolactone) (Messersmith and Giannelis, 1993), polyacrylonitrile (Blumstein, 1974), and polyfurfuryl alcohol (Bandosz, 1992).

Lan and Pinnavaia (1994) studied the intercalation of a polyamic acid into the galleries of a series of montmorillonites and the subsequent conversion of the polyamic acid to polyimide. The results indicated that the polyimide intercalates in large part as a monolayer and the composite exhibits enhanced barrier film properties, as judged from CO_2 permeation measurements. Although face-face clay layer aggregation is extensive, the clay-polyimide hybrid composite films exhibited greatly improved CO_2 barrier properties at low clay content. Less than 8.0 volume % clay results in nearly a ten-fold decrease in permeability rate. A self-similar or fractal dispersion of the clay platelets in the polyimide matrix may explain the barrier property enhancement.

In addition, the incorporation of low loading levels of clay into the polyimide hybrid results in a significant reduction in the permeability of water vapor, oxygen, and ethyl acetate vapor, as compared to the pure polyimide film. The results demonstrated a non-linear dependence of permeability on clay loading. The temperature dependency of the transport process, over the temperature ranges studies, followed well the Arrhenius relationship. Under humidified conditions, the polyimide film showed a loss in barrier property, while the polyimide-clay film showed an enhancement in the barrier properties to ethyl acetate vapor. (Gu, 1997)

The morphology or crystallization behavior of nylon 6/montmorillonite nanocomposites has been studied by means of wide-angle x-ray diffractive (WAXD), small-angle laser scattering (SALS), and differential scanning calorimeter (DSC). The nanoplastics of montmorillonite dispersed in the nylon-6 matrix were found to act as a nucleating agent. Surface modification of montmorillonite particles was found to increase adhesion between nylon-6 and montmorillonite, which prohibits the crystallization of nylon, thus leading to an increase in crystallization activation energy. (Li et al., 1997).

In order to improve the thermal stability and mechanical properties of polyimides, a series of polyimide/silica composite films, which ranged in silica content up to 45 wt%, were successfully prepared by sol-gel reaction of tetraethoxysilane in the presence of polyamic acid, a precursor of polyimide. The density, decomposition temperature and modulus increased with increasing silica content. In addition, the linear thermal

expansion coefficient of the silica in the composite films decreased, whereas tensile strength and elongation at break displayed a maximum with the change of silicate content. (Chen, et al., 1997).

Based on the results of these studies, polymer-clay nanocomposites processing has been developed for the plastics industry. Nanocor Inc., a branch of AMCOL International Corporation, has claimed that their unique, chemically modified clays, when added to polymers, form nanocomposites. Compared to the base polymer, the nanocomposites demonstrate improved heat resistance, as well as enhanced structural and barrier properties. Nanocor has partnered with plastic resin producers and users to develop the special technologies and products suitable for several different polymer types. Targeted applications being considered range from flexible and rigid barrier packaging to structural components for trucks and automobiles. Pilot plant facilities have been established to advance process operations and produce trial quantities of NANOMER®* nano-sized platelets. The initial commercial production of some products was launched in the second half of 1997. Nanocor received its first patent pertaining to the preparation of chemically modified clays and nanocomposites in September 1996. (Nanocor web page, 1997)

* NANOMER® is the trademark of Nanocor Inc.

Because of their unique properties, polymer-clay hybrids have been considered for a number of applications in both manufacturing and research areas, as reviewed below:

- Food Packaging

In 1997, Triton Systems (Triton Systems, Inc., 1997) proposed an innovative nanotechnology that would develop an inexpensive, recyclable, and mechanically durable material for a food tray with sufficient barrier properties to provide food with a three-year shelf life. A new generation of polymeric sheet stock material with a high barrier embedded glass structure, capable of being thermoformed into a retortable food-container, was to be produced. This unique and innovative technology involves embedding a highly elastic barrier glass structure within a polymer sheet stock during extrusion. This single-layered, recyclable food tray can replace the current non-recyclable co-extruded 3-layered tray. A reduction in energy and die costs may also be realized because of the use of a single extruder for processing of the single-layered tray. This technology has tremendous potential as a high gas and moisture barrier material in food packaging applications in the form of rigid and semi-rigid food containers, as well as flexible pouches. Other applications include airplane interiors, brakes, tires, fuel tanks, components in electrical and electronic parts, and under-the-hood structural components. Replacement of current filled-polymer systems in automobiles, and airplanes offers tremendous potential.

- Multi-chip Packaging Material

Polyimides are widely used for microelectronics because of their heat resistance, chemical stability, and superior electric properties. However, it would be desirable to reduce the cost and dielectric constant of the polyimide employed. Kim (1997) reported that a silica-polyimide hybrid could improve the electric properties and reduce the cost of the pure polyimide film. The structure of silica-polyimide composites, prepared as thin films, was studied by small-angle x-ray scattering and microscopy. Nanometer-scale composites were successfully obtained from ≤ 30% tetraethoxysilane-loaded mixtures with poly (amic diethyl ester) and poly (amic acid). The microstructure of the composite films, based on poly (amic diethyl ester) was not significantly affected by the inorganic particles, i.e., the structure of the homo-polyimide was maintained, while those based on poly (amic acid) showed changes in structure due to the growth of nanoparticles *in situ* during the sol-gel process.

- Electronic Industries

Momma (1997) reported that nanocomposites of vanadium pentoxide (V_2O_5) aerogel and conducting polymers have applications in the preparation of high performance intercalation materials for rechargeable lithium batteries. Vanadium pentoxide (V_2O_5) has been proposed as a cathode material in electric energy storage batteries, due to its high electrode potential and capacity. Aerogels of V_2O_5 (ARG) are materials characterized by high porosity with a solid phase thickness in the nanometer scale (10 ~ 50 nm). They were shown to be almost free of lithium diffusion limitation during the electrochemical insertion and release processes, because of the very short diffusion length of the intercalate cation in the V_2O_5 solid phase. Using a conducting polymer with a nanometer size structure was found to help enhance the electronic conductivity of the ARG. The addition of a nanometer thick conducting polymer layer covering to the vanadium penetrates covered structure, provides electronic conductivity throughout the ARG particle without loosing the merits of ARG. In this case, the polypyrrole coating exhibits electronic conductivity with ionic transparency. The resultant ARG-Polypyrrole nanocomposite material showed improved electrochemical performances compared to the bare ARG.

- Automobile industries

The Toyota researchers reported that the nylon-6-clay nanocomposites exhibited mechanical and thermal properties which were remarkably superior to those of the individual components. At a loading of 5.0wt% exfoliated clay, the tensile strength of the composite increased by 50% and the heat distortion temperature increased from 65 °C to 152 °C (Fukushima and Inagaki, 1987). Transmission Election Microscopy studies revealed that the improved performance observed was due to the formation of a nanoscopic composite. The nanocomposite immediately found application in the automobile industry, as the structural material of bumpers (Okada et al., 1990). According to a recent report (Usuki et al., 1995), it was found that a nylon 6-clay hybrid using montmorillonite was superior to the other types of clay minerals in mechanical properties. This was attributed to the montmorillonite interacting strongly with nylon 6 by ionic interaction.

- Material Industries

To evaluate the feasibility of controlling polymer flammability via a nanocomposite approach, Gilman et. al. (1997) have examined the flammability properties of nylon-6 clay-nanocomposites. The fire retardant (FR) properties of this new class of materials, organic-inorganic nanocomposites, were reported by the authors. The cone calorimeter data showed that the peak heat release rate (HRR), the most important parameter for predicting fire hazard, is reduced by 63 percent in a nylon-6 clay-nanocomposite containing a clay mass fraction of only five percent, as compared to the simple polyamide. Not only is this a very efficient FR system, but, it does not have the usual drawbacks associated with other FR additives. That is, the physical properties are not degraded by the additive (clay), instead they are greatly improved. Furthermore, this system does not increase the carbon monoxide or soot produced during the combustion, as many commercial fire retardants do. The nanocomposite structure appears to enhance the performance of the char through reinforcement of the char layer. Indeed, transmission electron microscopy (TEM) of a section of the combustion char from the nylon-6 clay-nanocomposite (five percent) shows a multilayered silicate structure. This layer may act as an insulator and a mass transport barrier slowing the escape of the volatile products generated as the nylon-6 decomposes.

3. The Barrier Improvement of Polyimide-clay Nanocomposites

Polyimides which exhibit excellent thermal, chemical and mechanical durability have attracted much attention for their potential use in gas separation processes. When montmorillonite was intercalated with the ammonium salt of 12-aminododecanoic acid, it dispersed at the molecular level into the polyimide matrix. Due to this unique structure, this polyimide hybrid exhibited high strength, high modulus, low thermal expansion coefficient and a low permeability coefficient. Only 2 wt % addition of montmorillonite reduced gas (water, O_2) permeability values to less than half of that of the non-clay loaded polyimide. (Okamoto et al. 1992)

Polyimides also have electronic, composite and adhesive applications. In these applications, it would be desirable to increase their moisture and organic vapor barrier properties and dielectric constant, since these properties of polyimides are not sufficient for advanced electronics use. As montmorillonite is composed of stacked silicate sheets, it has high gas barrier properties. Therefore, this polyimide-clay nanocomposite would be expected to exhibit enhanced barrier properties.

Montmorillonite is one of the clay minerals whose size is about 2000 Å in length and 10 Å in thickness. Recent studies evaluated the effect of the size of clay minerals on the barrier properties of the resultant polyimide-clay nanocomposites (Yano, 1997). Four different sizes of clay minerals were synthesized and compared. These clays consisted of stacked silicate sheets of about 460 Å (hectrite), 1650 Å (saponite), 2180 Å

(montmorillonite), and 12300 Å (synthetic mica), respectively in length and 10 Å in thickness. Yano (1997) found that the longer the length of the clay platelet, the more effectively the barrier properties of the polyimide were improved. In the case of the polyimide-mica hybrid, only 2 wt % addition of synthetic mica reduced the permeability coefficient of water vapor to a value less than one-tenth of that of ordinary unfilled polyimide.

The earliest studies on the barrier properties of polyimide-clay nanocomposites were carried out by the Toyota group (Fukushimaand and Inaganki, 1987, 1988). They found that the addition of only 2 wt% montmorillonite, reduced the permeability coefficients of various gases to values less than half of those of the ordinary unfilled polyimide (Yano, 1993). Furthermore, it has been suggested that nearly complete dispersion of the 10-Å-thick clay layer is needed to optimize the aspect ratio of the filler (the aspect ratio is defined as the ratio of the length of a face of a filler plate to the thickness of the filler plate), which in the case of montmorillonite can reach a value of 200 (Yano, 1993). Lan and Pinnavaia (1994) showed that similar composites, with an aspect ratio of 192, had enhanced CO_2 barrier properties. To describe the mechanism of the barrier property enhancement of polyimide-clay nanocomposites, Lan and Pinnavaia (1994) compared the structural difference between exfoliated and intercalated polyimide-clay hybrids. In the exfoliated structure, the single clay layers act as filler elements. The aspect ratio of the individual clay plates and the filler loading were found to determine the barrier property improvement. And for the intercalated structure, the clay fractal aggregates, and not single layers, function as filler elements. The formation of the fractal

clay structure for natural clay minerals is due to a water swelling effect. When water molecules have been pre-intercalated into the clay galleries and then evaporated from the system, they tend to form a water domain region. This causes the clay layers to slip and change their stacking pattern from turbostratic to a staircase fashion. During the synthesis of the polyimide-clay nanocomposites, a rearrangement of the clay stacking occurs to form the fractal structure of the clay within the polyamic acid matrix during the pre-intercalation process. After further heating, the clay fractal structure will simply remain because of the low mobility of the preformed polymer chains.

While various researchers have proposed different mechanisms to account for the barrier property enhancement of polyimide-clay nanocomposites, the observed non-linear dependence of the diffusion coefficients as a function of clay loading and the very low content of the inorganic phase, is crucial in developing light-weight composites of enhanced barrier properties.

In an earlier study, Gu (1997) determined the permeability of water vapor, oxygen, carbon dioxide, and ethyl acetate vapor through the same polyimide-clay nanocomposite films. These permeability values were determined with the MOCON Permatran-W, Ox-Tran 200, Permatran C-IV, and the Aromatran 1A permeability test systems, respectively. Gu (1997) found that the mass transfer process for the respective penetrants, i.e. water, CO_2 and O_2, is highly dependent on the clay loading level and exhibited a non-linear dependency with the respect to the decrease in permeability. With a clay loading level of 2.5 % (v/v), the permeability coefficients to H_2O, O_2 and CO_2

were reduced to 39 %, 47 % and 54 % of the permeability value of the pure polyimide film, while the permeability coefficients of the 5% (v/v) clay loading film were deceased by nearly 70 %, when compared to the single polyimide. Gu (1997) also found that the temperature dependency of the oxygen transport process followed well the Arrhenius relationship, over the testing range evaluated (0 °C - 30 °C). The obtained activation energies for the pure polyimide and the 2.5 % v/v polyimide-clay film were 16.9 KJol/mol and 19.6 KJol/mol, respectively. Furthermore, when ethyl acetate vapor was evaluated as a penetrant, the following results were obtained. a) The 2.5 % v/v polyimide-clay nanocomposite film under dry conditions showed an 85 % reduction in the permeability coefficient, as compared to the polyimide film without clay loading. b) Within the test temperature range from 15 °C to 30 °C, the effect of temperature on the permeability coefficient is minimal. Less than 3200 Pa ethyl acetate vapor pressure, the activation energies for the pure polyimide and the 2.5 % v/v polyimide-clay film are 7.1 KJol/mol and 4.1 KJol/mol, respectively. c) Over an ethyl acetate vapor pressure range from 1700 Pa to 3200 Pa, the permeability coefficient appeared to be independent of vapor concentration. There was no indicated effect of penetrant vapor pressure on the activation energies for the polyimide-clay composite film, while the activation energy of the pure polyimide showed a minimal dependency on penetrant concentration. d) When water vapor (50% RH) was introduced to the test system, the permeability coefficient value of the pure polyimide film doubled as compared to that obtained under dry conditions. However, the permeability coefficient for the polyimide clay nanocomposite (2.5 % v/v) film under humidified conditions showed a decrease of approximately 50 % when compared to permeability coefficient obtained under dry conditions.

Ideal Diffusion and Sorption of Organic Vapor in Glassy Polymers

Diffusion is the net transport of matter in a system, by means of random molecular motion. This results in the removal of chemical potential differences in a system and eventually produces a uniform state of equilibrium, if the boundary conditions are not held constant for a permeation experiment. (Hopfenberg and Stannett, 1973)

Frequently the rate of diffusion (J) is proportional to the concentration gradient, although the proportionality constant, known as the diffusion coefficient, may be a function of the diffusant concentration in the polymer:

$$J = -D(c)\frac{\partial c}{\partial x} \qquad (1)$$

This is Fick's first law of diffusion and it has been found experimentally to represent diffusion in many systems. Based on Fick's first law, for vapors above their critical temperature, the diffusion coefficient is independent of penetrant concentration. Fick's second law may be derived from Fick's first law:

$$\frac{dc}{dt} = \frac{\partial}{\partial x}\left(D(c)\frac{\partial c}{\partial x} \right) \qquad (2)$$

When the boundary conditions are fixed, such that a steady-state diffusion flux is maintained, equation (1) can be used to calculate the steady state permeability, defined as the flux per unit pressure gradient across a polymer membrane of unit thickness; assuming Henry's law to describe the gas-membrane equilibrium. Henry's law simply states that the concentration of penetrant in the polymer, C, is directly proportional to the gas partial pressure, p, to which the polymer is exposed:

$$C = S\ p \qquad (3)$$

The relationship between the permeability, diffusion, and solubility coefficients can be described by:

$$P = D\ S \qquad (4)$$

where P is the steady state permeability coefficient, cc[STP] · m/m^2 · pa · sec

D is the concentration independence diffusion coefficient, m^2/sec

C is the solubility of vapor absorbed in the polymer

or concentration of vapor in the polymer, cc[STP]/cc polymer

S is the solubility coefficient, cc[STP]/cc · pa^{-1}

p is the vapor partial pressure, pa

Strictly idealized behavior results not only from Fickian diffusion but also additionally from a Henry's law description of solution.

Non-ideal Sorption and Diffusion of Organic Vapor in the Glassy Polymers

The magnitude of the negative enthalpies of sorption of organic vapors by polymers reported by Barrer (1957) were inconsistent with the sorption theories of Henry's law and led Barrer to suggest a dual-mode, concurrent sorption mechanism for glassy polymers, namely ordinary dissolution and 'hole' filling.

Michaels *et al.* (1963) also reported and proposed that a two-mode sorption model of ordinary dissolution and adsorption in microvoids ("holes") for gas sorption in glassy amorphous polymers. The authors (Michaels *et al.*, 1963) assumed that the total concentration of the sorbate in the polymer, C, consisted of two thermodynamically distinct molecular populations; molecules 'adsorbed' in the 'holes' or microvoids, C_H, and molecules dissolved in the amorphous polymer matrix, C_D, as shown in equation (5):

$$C = C_H + C_D \qquad (5)$$

The concentration C_H was described by a Langmuir isotherm:

$$C_H = \frac{C'_H bp}{1 + bp} \qquad (6)$$

and the concentration C_D by Henry's law:

$$C_D = k_D \cdot p \qquad (7)$$

where C'_H = hole saturation constant cc[STP]/cc polymer

b = hole affinity constant (pa^{-1})

p = vapor partial pressure (pa)

k_D = Henry's law constant for dissolution in the amorphous matrix,

cc[STP]/cc · pa^{-1}

The equilibrium concentration for the "dual mode sorption model" can be described by:

$$C = C_H + C_D = \frac{C'_H bp}{1 + bp} + k_D p \qquad (8)$$

This model was applied by Okamoto et al.(1992) to the sorption isotherm of water vapor by a polyimide film and gave an excellent fit of water vapor sorption by the glassy, amorphous polymer. The isotherm for this sorbate/polymer sorption was described by the following expression:

$$C = \frac{0.01356\ p}{1 + 2.26 \times 10^{-3} p} + 6.32 \times 10^{-3} p \qquad (9)$$

It is instructive to show the two limiting cases from the dual mode sorption model.

At **low** partial pressure ($b\,p << 1$), equation (8) reduces to :

$$C = C'_H\, b\, p + k_D\, p \qquad (10)$$

For many glassy polymer systems, $C'_H b$ is significantly larger than k_D. Therefore reducing the equation (10) to:

$$C = C'_H \, b \, p \qquad (11)$$

At **high** partial pressure, $b\,p >> 1$ which reduces the equation (8) to:

$$C = C'_H + k_D p \qquad (12)$$

At sufficiently high pressure the term C'_H / p becomes negligible as compared to k_D, therefore indicting that the available 'holes' have become saturated and that ordinary dissolution dominates. Later investigations by Vieth et al. (1966) on glassy polymers indicted that the gas molecules are sorbed in the "hole" site, only as monolayers.

The dual-mode sorption model therefore predicts that an isothermal plot of *C versus p* will consist of a low-pressure linear region and a high-pressure linear region connected by a nonlinear region. So, k_D can be obtained from the slope of the sorption isotherm at high pressures. By subtracting the solubility of the normally dissolved gas, C_D, from the total solubility C, the solubility of the sorbate in the microvoids, C_H, can be calculated at each partial pressure:

$$C_H = C - C_D = C - k_D p \qquad (13)$$

Once C_H as a function of p has been determined, it can be tested in terms of the assumed Langmuir model:

$$C_H = C'_H b p /(1 + b p) \qquad (14)$$

Equation (14) can be rearranged to:

$$\frac{p}{C_H} = \frac{1}{C'_H b} + \frac{p}{C'_H} \qquad (15)$$

Therefore, to test whether a single Langmuir expression fits the data for the hole-fitting process a least-mean-squares plot of p/C_H *versus* p is made and is checked for linearity. The constants C'_H, and b can be determined from the slope and y-intercept of such a Langmuir plot.

Model for the path of a diffusing gas through the polyimide/clay nanocomposite

The significant reduction of the permeability coefficients of the polyimide-clay nanocomposite films, as compared to the non-clay loading control, was explained by the increase of the total path of the diffusing gas through the structure. As clay is composed of stacked silicate sheets, it exhibits high gas barrier properties. The diffusing gas has to go along the length of the clay instead of the width, which is a hundred time less than lengthwise. Therefore, the total path of the diffusing gas will increase. If a plate of length **L** and thickness **W** is dispersed parallel in a polymer matrix, the tortuosity model for the path of a diffusing gas through the polyimide clay nanocomposite is shown by Figure 2 (Nielsen, 1967):

For montmorillonite, length of a clay L = ~ 2000 Å, width of a clay W = 10 Å. The value of L was determined from transmission electron micrograph (TEM) (Yano et al., 1993).

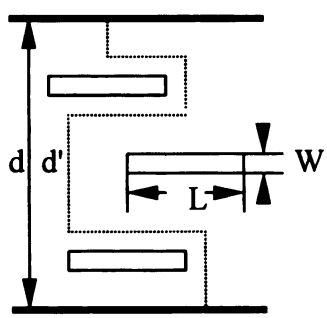

Figure 2 A model for the path of a diffusing gas through the polyimide clay nanocomposite.

Total path of a diffusing gas

$$d' = d + d\,L\,V_f / 2W \tag{16}$$

where d is the thickness of a test film and v_f is the volume fraction of a clay.

Tortuosity factor

$$\tau = d'/d = 1 + (L / 2W)\, v_f \tag{17}$$

where v_f represents a volume fraction of a clay plate. The permeability coefficient ratio is given by:

$$\frac{P_c}{P_p} = \frac{1}{\tau} = \frac{1}{1 + (L/2W)v_f} \tag{18}$$

where P_c and P_p are a permeability coefficient of composite and polymer matrix, respectively.

According to the equation above, the permeability coefficient ratio should be smaller as aspect ratio (ratio of length versus width) of plate becomes bigger.

Materials and Methods

A. Materials for synthesis of clay/polyimide Nanocomposite

1. Natural montmorillonite

Source clay mineral Depository
University of Missouri, Columbia, Missouri
Unit cell: $Na_{0.86}$ [$Mg_{0.86}$ $Al_{5.14}$ ($Si_{8.00}$) O_{20} $(OH)_4$]

2. 4, 4' - diaminodiphenylether (4, 4' - ODA)

Aldrich Chemical Co. (Milwaukee, WI)
Molecular Weight: 200.24
Melting point: 190-192 °C
Purity: 99%

3. Pyromellitic Dianhydride (PMDA)

Chriskev Company, Inc. (Leawood, KS)
Molecular Weight: 218.12
Melting Point: 286.7 °C
Purity: 99 %

4. Dimethylacetamide (DMAC)

Aldrich Chemical Co. (Milwaukee, WI)
Molecular Weight: 87.12
Melting Point: - 20 °C
Boiling Point: 164 ~ 166 °C
Purity: 95 %

5. Octadecylamine (18 A)

Aldrich Chemical Co. (Milwaukee, WI)
Molecular Weight: 269.52
Melting Point: 55 ~ 57 °C
Purity: 99 %

B. Materials for Sorption tests

1. Ethyl acetate (CH_3-COO-C_2H_5)

   J. T. Baker Chemical Co. (Phillipsburg, NJ)
   Analytical Reagent grade
   Molecular Weight: 88.11
   Boiling Point: 77.2 ± 0.5 °C
   Purity: 99.9 %

2. Ethylene Glycol (HO-CH_2-CH_2-OH)

   J. T. Baker Chemical Co. (Phillipsburg, NJ)
   Laboratory grade
   Molecular Weight: 67.07
   Boiling Point: 197 ± 0.5 °C
   Purity: 100 %

3. Acetonitrile (used as a solvent when preparing standard solutions for construction of an ethyl acetate calibration curve)

   EM Science, Gibbstown, NJ
   Laboratory grade
   Molecular weight: 41.05
   Boiling point: 81.2 ± 0.5 °C
   Purity: 99.8 %

4. Nitrogen gas (carrier gas of the sorbate vapor)

   AGA Gas, Inc., Cleveland OH
   Dry grade nitrogen: 99.98%

C. Synthesis of Clay-Polyimide Nanocomposite Film

In the present study, montmorillonite/polyimide nanocomposites were prepared in a two step process involving condensation polymerization, followed by a cyclodehydration reaction, as described by Lan (1994).

A flow chart of the synthesis of the polyimide-clay nanocomposites is depicted in Figure 3. Polyamic acid was synthesized by the condensation reaction between 4,4'-diaminodiphenylether and pyromellitic dianhydride in dimethyl acetamide (DMAC). An amount of pyromellitic dianhydride was slowly added to the 4,4'-diaminodiphenylether/ DMAC solution with vigorous stirring at 15 - 20 °C and kept stirring for 1 hr at room temperature. The final polyamic acid solution has a concentration of 7 wt%.

Polyamic acid-clay intercalates were prepared by reaction of the desired organoclay (2 -10 wt%) with the polyamic acid solution at 25°C. The clay suspension, in polyamic acid/ DMAC solution, was then vigorous stirred for 24 hrs, followed by a 2hr settle down period. Allowing the polyamic-organoclay suspensions to dry on a clean glass plate yielded self-supporting films. The air-dried polyamic acid-clay films were heated at 1°C/min to 300 °C and kept at 300 °C for 3 hrs to form the cured polyimide-clay hybrid composites.

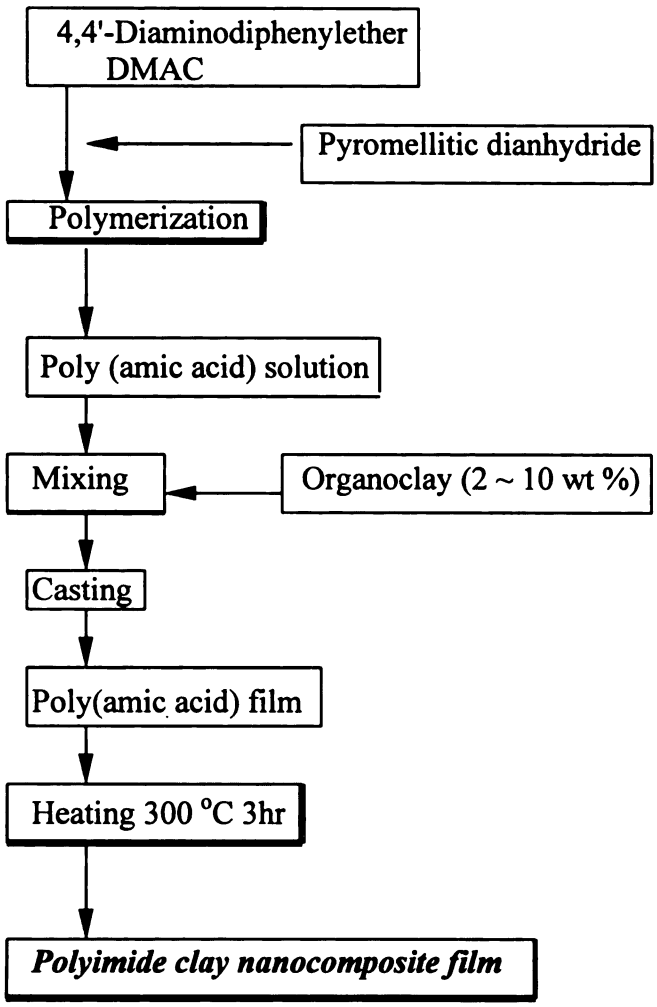

Figure 3 Synthesis of polyimide clay hybrid.

D. Cahn 2000 Electrobalance

Sorption experiments conducted using the gravimetric technique are usually carried out at equilibrium vapor pressure and employ an apparatus that continuously records the weight gain or loss of a polymer sample as a function time. A recording electrobalance, such as the Cahn 2000, is commonly used for such studies.

The Cahn 2000 is a very sensitive weighting instrument and is designed to measure weights up to 3.5g. It has a 0.01mg resolution and a 0.02mg precision, for a measuring scale of 100.00mg. The electrobalance can be described as a torque-to-current converter. The apparatus consists of a balance beam mounted to, supported by and pivoting about the center of a taut ribbon; a torque motor coil, located in a permanent magnetic field and also mounted to the taut ribbon; sample suspension fixtures; a beam position sensor system; and controls, circuitry and indicators.

When conducting a sorption measurement by the continuous flow method, the polymer sample is suspended from the arm of the electrobalance, and a sorbate of constant concentration is continuously flowed through the sample hangdown tube. The sorbate vapor is produced by bubbling pure nitrogen gas through the liquid sorbate. This can be achieved by constructing a vapor generator system, consisting of an Impinger Bubbler, containing the organic liquid. As the weight of the polymer test sample changes, a torque is produced about the axis of rotation. The electrobalance effectively measures the amount of electric current needed by the torque converter to maintain the

balance beam in a level position. By calibrating the electrobalance using calibration weights, the change in electric current can be related to weight change of the polymer sample. By interfacing the electrobalance control unit to a computer, the polymer sample's change in weight can be continuously recorded, as a function of time.

E. Gravimetric Sorption Method

Sorption studies were conducted on a Cahn 2000 electrobalance (Cahn Instruments, Inc., Cerritos, CA) by the continuous flow method. A schematic of the test system is shown in Figure 4. A polymer sample weighing approximately 25 ~ 60 mg was suspended from the arm of the electrobalance. A sorbate vapor stream of constant concentration was produced by bubbling pure nitrogen gas through the liquid sorbate. This was achieved by constructing a vapor generator system, consisting of an Impringer Bubbler, $24/40, 25ml (Ace Glass Inc. 1430 N West BLVD, Vineland, NJ 08360), which contained the organic liquid. The Impringer Bubbler, or sparger unit, was maintained in a constant temperature control bath (NESLAB, Endocal RTE-100, Refrigerated Bath/Circulator, Neslab Instruments, Inc. Newington, NH) as a means of controlling the vapor pressure of sorbate delivered to the hangdown tube of the electrobalance unit.

To provide insight into the concentration dependency of the mass transfer process, seven vapor activity levels were evaluated: 0.15, 0.21, 0.27, 0.34, 0.44, 0.55,0.68.

Flow meters (Cole Parmer, Chicago, IL) and needle valves (Nupro 'M' series, Nupro Co., Willoughby, OH) were used to regulate the gas flow and indicated a constant flow rate. The sorbate uptake was continuously recorded with a computer, until steady state was reached.

The test gas delivered can be a certified gas or sparging gas. In this study, a sparging gas was used. The organic liquid is added to the sparger, and a carrier gas is passed through the liquid in such a manner so as to obtain a known and stable concentration of the permeant in the test gas stream. The test gas stream is connected directly to the test gas inlet of the hangdown tube. Test gas flows were normally set at 15 cc/min.

When the temperature controller bath is set at a specified temperature, the organic liquid inside the sparger generates a fixed and constant saturation vapor pressure at that specific temperature. It is suggested that the sparging system should be maintained at a temperature below ambient so as to insure that there is no condensation in the delivery lines. In this study, the bath was set at temperatures ranging between -10 °C to 16 °C, depending upon the desired vapor activity. The resultant organic vapor partial pressure in the hangdown tube is equal to the saturation vapor pressure generated in the sparger. The conclusion is based on the following reasoning (Hernandez, 1994):

The vapor pressure is generated at T_A (point A), while the film is evaluated within the test system maintained at a higher temperature T_B (point B). The parameters of partial pressure, concentration and volume for the organic vapor generator and test conditions are denoted as p_A, p_B, C_A, C_B, V_A and V_B, respectively.

Assumption:

i) At point A and B, the mass flows are equal.

Therefore, $M_A = M_B = M$, where M is the mass flow (mass/time).

ii) The organic vapor pressure is usually low, therefore the mass flow consists primary of nitrogen (N_2). For this case, it can therefore be assumed that the organic vapor behaviors as an ideal gas. In follows then, that $F_B = F_A * T_B / T_A$, and by definition:

$C = M / F$, where F is the gas flow rate (volume / time).

So, the concentration ratio is $C_B / C_A = T_A / T_B$

When expressing C or p by the ideal gas law, at point A:

$p = nRT/v = R/MW * m/v * T = R/MW * C * T$

$p_B / p_A = C_B T_B / C_A T_A$

$p_B = p_A * 1/C_A T_A * C_A T_A/T_B * T_B = p_A$

So, at point A and B:

- Temperatures are different
- Mass flows are equal
- Flow rates are different
- Partial pressures are equal

The composition of the vapor stream was determined by using a high performance, gas tight syringe (Hamilton 1750, Supelco Inc., Bellefonte, PA) to take samples from the sampling port located on the hangdown tube and performing gas chromatography (GC) analysis. All of the gravimetric sorption studies were conducted at a temperature of 23 ± 1 °C.

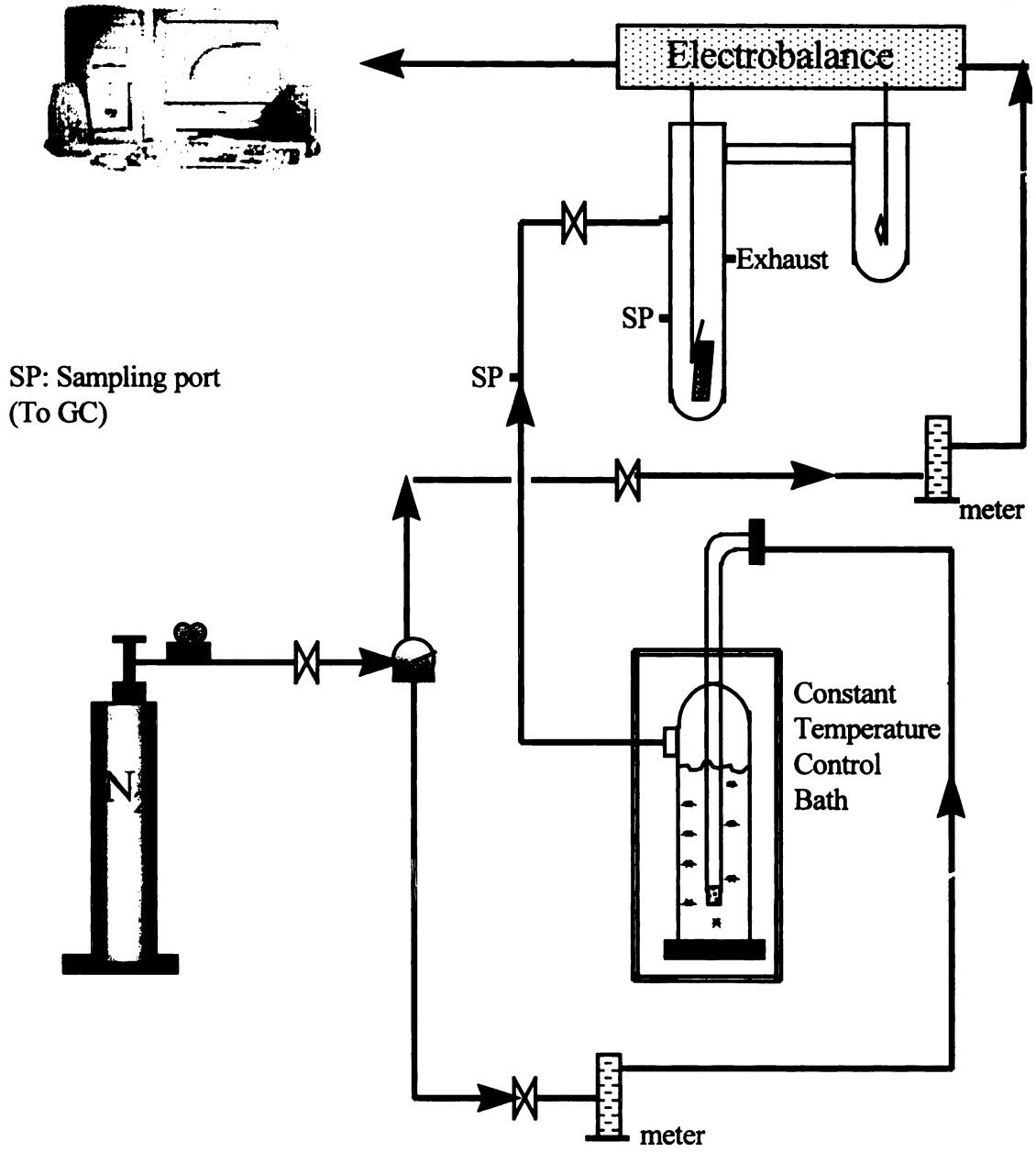

Figure 4 Schematic of Gravimetric Sorption Experimental

F. Gas Chromatographic Analysis

Gas chromatographic analyses were performed using a Hewlett-Packard 5890A gas chromatograph, equipped with a dual flame ionization detector and interfaced with a Hewlett-Packard 3395 integrator for quantification (Avondale, PA). The column used in this study was a Supelcowax 10 fused silica capillary column (60m, 0.25mm ID, 0.25μm film thickness) (Supelco Inc., Bellefonte, PA). A detailed summary of the procedure for calibration curve construction is presented below:

Materials:

- 25mL and 100mL volumetric flasks with stoppers
- 500μL high performance gas tight syringe
- 1 and 5mL sterile pipettes with automatic pipette fixtures
- Lab grade ethyl acetate and acetonitrile

Procedure:

To determine the relationship between area response and the ethyl acetate quantity injected, a calibration curve was constructed using the following procedure:

1. Prepare a 1000ppm (v/v) standard stock solution

   Using a high performance gas tight syringe, add 0.1mL of ethyl acetate to a 100ml volumetric flask. Fill to 100mL with acetonitrile. Stopper the flask and swirl to ensure proper mixing.

2. From the 1000ppm stock solution, prepare 25mL standard solutions of the following concentrations: 10, 20, 40, and 80ppm (v/v).

   To the four 25mL volumetric flasks, add 0.25, 0.5, 1.0 and 2.0mL of the 1000ppm stock solution, respectively. Fill to 25mL with acetonitrile. Stopper the flasks and swirl to ensure proper mixing.

3. Using the GC settings presented in Table 1, analyze each standard solution by injecting a 1μL aliquot directly into the gas chromatograph for quantification. Repeat until a consistent response value is obtained for each concentration.

Table 1. Gas chromatography conditions used for ethyl acetate quantification

Column	Supelcowax 10
Injection temperature	220 °C
Detector temperature	250 °C
Initial temperature	100 °C
Initial time	9 min
Rate	7.5 °C/min
Final temperature	220 °C
Final time	15 min
He (carrier gas)	7.0 mL/min
H_2	40 mL/min
Air	400 mL/min
Nitrogen (make-up gas)	30 mL/min

4. Plot the average area response value obtained for each concentration as a function of the ethyl acetate quantity injected. The injected quantity of ethyl acetate can be calculated from the following expression:

$$q_i = v_i \times c \times 0.902 \ {}^{g}/_{mL} \qquad (19)$$

Where q_i represents the quantity injected, v_i is the injection volume, c is the concentration of the standard solution (v/v), and 0.902 g/mL is the density of ethyl acetate. The ethyl acetate calibration curve is presented in Figure 5:

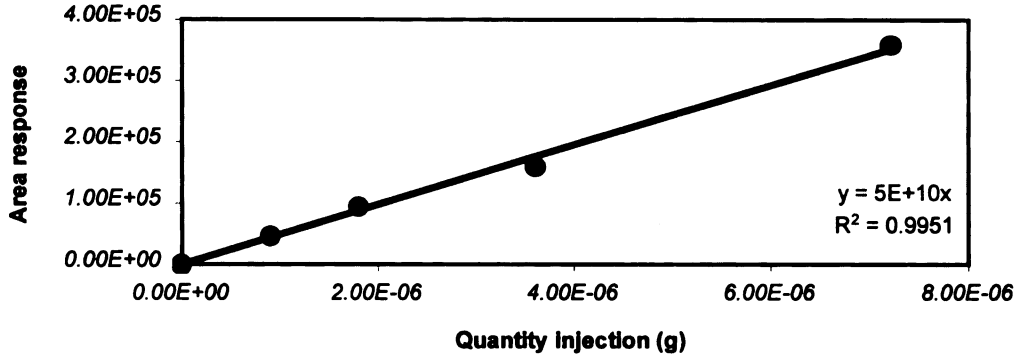

Figure 5. Ethyl acetate calibration curve

5. Using linear regression, determine the slope of the standard curve. Take the inverse of this value to obtain the ethyl acetate calibration factor.

A calibration curve was constructed to determine the relationship between area response and ethyl acetate quantity injected. Retention times for ethyl acetate and acetonitrile were found to be 7.2 and 8.4 minutes, respectively. In addition, the saturation vapor pressure of ethyl acetate at 23 °C was experimentally determined using gas chromatographic analysis. The following is the method used to calculate the ethyl acetate vapor activity levels employed in this study.

Materials

- 500μL gas tight syringe
- 50mL crimp seal vials
- Aluminum crimp cap
- Teflon coated septa seals
- 5mL sterile pipettes with automatic pipette fixtures
- Lab grade ethyl acetate

Procedure

The saturation vapor pressure and the vapor activity of ethyl acetate were experimentally determined using the following procedure:

1. Add 10mL of ethyl acetate to each vial and seal using a Teflon coated septa seal and an aluminum crimp cap.

2. Store the sample at 23 ^{o}C for one week, to allow the vial headspace to equilibrate,

3. Using the same GC conditions as the calibration curve in Table 1, determine the ethyl acetate saturation vapor pressure within the headspace by withdrawing a 50μL aliquot and injecting the sample directly into the gas chromatograph for quantification.

4. Determine the ethyl acetate saturation vapor pressure from the ideal gas law:

$$p\,V = n\,R\,T \tag{20}$$

5. Determine the vapor activity of the ethyl acetate test vapor.

Using GC conditions identical to those described above, determine the vapor pressure of the test ethyl acetate vapor by withdrawing a 50μL aliquot from the vapor stream sampling port and injecting the sample directly into the gas chromatograph for quantification. Vapor activity is determined from the following expression:

$$a_v = p_i / p_s \tag{21}$$

where a_v represents the vapor activity, p_i is the test vapor partial pressure of ethyl acetate, and p_s is the saturation vapor pressure of ethyl acetate.

The saturation vapor pressure value obtained from the literature (see appendix A) was 85.7 mmHg at 23 °C. The ethyl acetate vapor activity for the ethyl acetate permeant determined experimentally was compared with the values obtained from the literature (Appendix A) and are summarized in Table 2. The average percent deviation from the experimental was 3.3 % below the values obtained from the literature. The variation between the two procedures can be attributed to a number of factors, such as deviation of the permeant from the ideal gas law at or near the saturation point of the vapor, as well as errors introduced by the gas chromatography procedure and errors involved in the possible condensation in the test system.

Table 2. Comparison of the ethyl acetate vapor activity in the hangdown tube obtained by the experimental and literature.

Bath Temperature (°C)	*System vapor activity* obtained from literature	*System vapor activity* determined from experimental	Deviation based on the literature data
-10	0.150	0.15	0 %
-4	0.218	0.21	3.7 %
0	0.284	0.27	4.9 %
4	0.361	0.34	5.8 %
8	0.453	0.44	3.0 %
12	0.566	0.55	2.8 %
16	0.700	0.68	2.9 %

G. Calculation of diffusion coefficient

When a polymer sample of known shape and size, which is at an initially equilibrium state (uniform penetrant concentration), is suddenly exposed to an atmosphere of constant penetrant vapor pressure, the sample weight changes with time towards the sorption equilibrium value, according to kinetics governed by the penetrants diffusion coefficient. For dense polymeric materials such as polyamides, polyimides and polyethylene terephthalate, surface sorption is generally considered to be negligible, when compared with the sorption levels in the bulk polymer. As polyimide films are quite dense and uniform, a vapor absorption in the bulk materials is assumed. (Perrin et al., 1996)

If M_t denotes the total amount of the diffusing substance which has entered a flat sheet at time t, and M_∞ (or M_{ss}), the corresponding quantity after infinite time, the change in the mass of the sample, as a function of time, is given by: (Crank 1975)

$$\frac{M_t}{M_\infty} = 1 - \sum_{n=0}^{\infty} \frac{8}{(2n+1)^2 \pi^2} \exp\left[\frac{-D\pi^2(2n+1)^2 t}{l^2}\right] \qquad (22)$$

where D is the diffusion coefficient (m^2/s), ℓ the film thickness (m) and t is time (s). This equation is valid when the vapor penetrates bi-directionally in the material with a constant diffusion coefficient from both planer surfaces. If the film was bonded to an impermeable substrate (aluminum sheet) or vapor penetrates unidirectionally in the film from one surface, the thickness value in equation (22) is double that of the true sample.

As the sample films were thin sheets (thickness less than a hundredth of the width or length), penetrant sorption by the edges was assumed to be negligible, when compared with that by the plane surfaces.

In the case of sorption of vapors or condensable gases, the diffusion may progress locally at different rates due to the dependence of the diffusion coefficient on the local concentration. The dependence, known as the 'plasticization' effect on the polymer by the penetrant, is caused by an increase in the mobility of polymer segments with the local penetrant concentration. (Perrin et al., 1996)

To solve numerically Fick's second law equation, a trial-and-error method is typically employed to fit the experimental kinetics by varying the values of the parameters of the concentration dependence law. The simplest law, the one in which diffusion is Fickian with a constant value for the diffusion coefficient, is tested first. This is based on the assumption that the value of the diffusion coefficient can be calculated by different approximation methods, such as the method of half-sorption time $t_{1/2}$, or by a method using a transform of equation (22), with only the first term of the series. Nevertheless, with such methods, it is not possible to check the validity of the assumption of a constant diffusion coefficient. In this study, equation (22) was used for the fitting of the entire curve by the "Least square curve fitting method". A statistical treatment of the data $\sum[(M_{calc.} - M_{exp.})^2]$ showed that the total departure of the calculated from the experimental values should be minimized in order to obtain a good fit of the experimental data.

1) "half sorption time" method

Diffusion coefficient values, D, can be estimated using the following expression derived by Ziegel (1969):

$$D = 0.049 \frac{l^2}{t_{1/2}} \qquad (23)$$

On the assumption that the diffusion process followed Fickian sorption behavior, this equation can only be used when there is a good agreement between the experimental and theoretical sorption profiles. Estimation of $t_{1/2}$ is illustrated in Figure 6 for the penetrant/polymer system of ethyl acetate (a = 0.68) and the non-clay loading polyimide film.

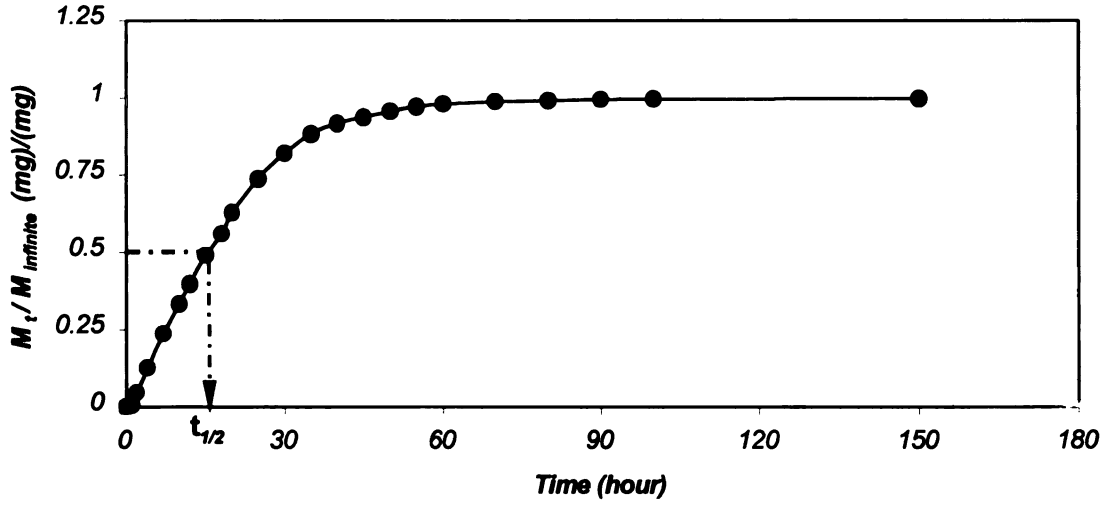

Figure 6 Half sorption time determined by sorption profile of 0.675mil non-clay polyimide film at ethyl acetate vapor activity a = 0.68 and T = 23 °C. ($t_{1/2}$ = 15.3 hours, D = 2.58 x 10^{-16} m^2/sec)

2) Gauss-Newton curve fitting method

Equation (22) can be used for fitting the entire sorption curve, based on the "Gauss-Newton curve fitting" method. In this procedure, diffusion coefficient values are selected and for each selected D value, a value of M_t is calculated from Equation (22) for each data point (n) on the sorption curve. Statistical treatment of the data $\sum[(M_{calc.} - M_{exp.})^2 / ((M_{calc.})^2 \cdot n)]$ showed the average relative departure of the calculated values from the experimental values. The best estimated D values can be determined by the least sum of the $\sum[(M_{calc.} - M_{exp.})^2 / ((M_{calc.})^2 \cdot n)]$. A value less than 1% is considered to be a likely good fit of the data to the theoretical equation (Perrin, 1996). A typical plot of the statistical treatment of the data $\sum[(M_{calc.} - M_{exp.})^2 / ((M_{calc.})^2 \cdot n)]$ is presented in Figure 7, where the sum of $\sum[(M_{calc.} - M_{exp.})^2 / ((M_{calc.})^2 \cdot n)]$ is plotted as a function of selected diffusion coefficient values. Here the diffusion coefficient giving the lowest value of $\sum[(M_{calc.} - M_{exp.})^2 / ((M_{calc.})^2 \cdot n)]$ is assumed to give the best fit of the experimental data to Equation (22).

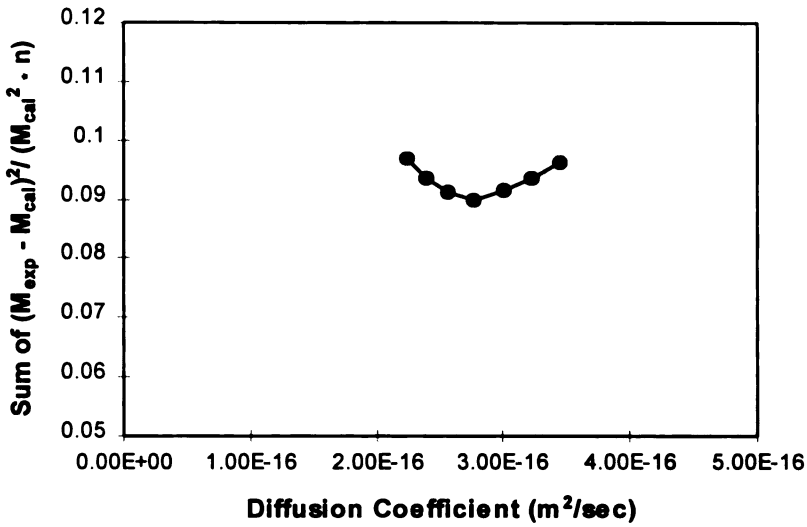

Figure 7. $\sum[(M_{calc.} - M_{exp.})^2 / ((M_{calc.})^2 \cdot n)]$ as a function of the best estimated diffusion coefficient value for the system of 0.675mil non-clay polyimide film at ethyl acetate vapor activity a = 0.68 and T = 23 °C. ($D_{best} = 2.8 \times 10^{-16}$ m^2/sec)

3) Least square method

Equation (22) can also be used for fitting the entire sorption curve, based on the least square method. For the least square curve fitting method, diffusion coefficient values are selected and for each diffusion coefficient value selected, values of M_t are calculated by solution of Equation (22). Statistical treatment of the data $\sum[(M_{calc.} - M_{exp.})^2]$ shows the total departure of the calculated values from the experimental values. The best estimated D value is determined from the minimum sum of the squares value, which is considered to be the likely best fit. A typical graphical treatment is presented in Figure 8, where the sum of squares is plotted as a function of the selected diffusion coefficient values.

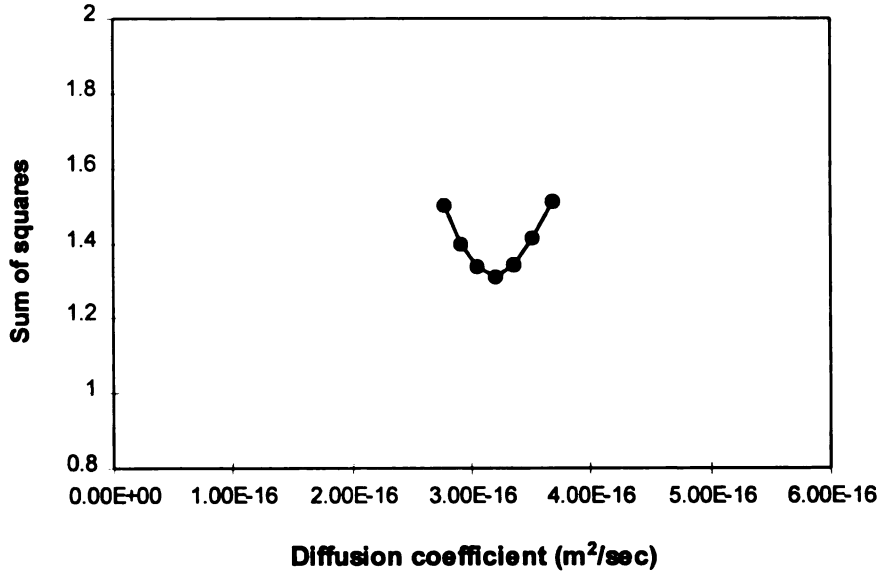

Figure 8. $\sum[(M_{calc.} - M_{exp.})^2]$ as a function of the best estimated diffusion coefficient value for the system of 0.675mil non-clay polyimide film at ethyl acetate vapor activity a = 0.68 and T = 23 °C. ($D_{best} = 3.2 \times 10^{-16}$ m^2/sec)

4) "Consistency for continuous flow" method

The consistency test for continuous flow permeability experimental data has been described in detail by Gavara and Hernandez (1993) and is summarized briefly below.

The permeation rate or permeant flux at any time F_t during the transient state portion of the permeability experiment, varies from zero at time zero, up to the value F_∞ reached at steady state. This is described by the following expression (24):

$$\frac{F_t}{F_\infty} = \frac{4}{\sqrt{\pi}}\left(\sqrt{\frac{l^2}{4Dt}}\right)\sum_{n=1,3,5\ldots}^{\infty}\exp\left(\frac{-n^2l^2}{4Dt}\right) \qquad (24)$$

where F_t/F_∞ is the permeant flux ratio. F_t is the permeant flux at time t, and F_∞ is the permeant flux at steady state. In this equation, D is assumed to be time and concentration independent. For short times, the first term of the convergent series in Equation (24) gives a good description of the permeation process from t = 0 up to the time when 95% of the steady-state flow has been reached. Equation (24) is then simplified to read:

$$\varphi = \frac{F_t}{F_\infty} = \frac{4}{\sqrt{\pi}}\left(\sqrt{X}\right)\ e^{-X} \qquad (25)$$

where φ represents F_t/F_∞ in Equation (25) and $X = \ell^2/4Dt$. By using a Newton-Raphson method, the value of X can be calculated for each value of t and the diffusion coefficient D can be obtained from the slope of 1/X versus t. The plot of 1/X versus time is expected to be a straight line and to intercept the ordinate axis at zero. This is illustrated in Figure 9 for the ethyl acetate (a = 0.68) / non-clay loading polyimide film system.

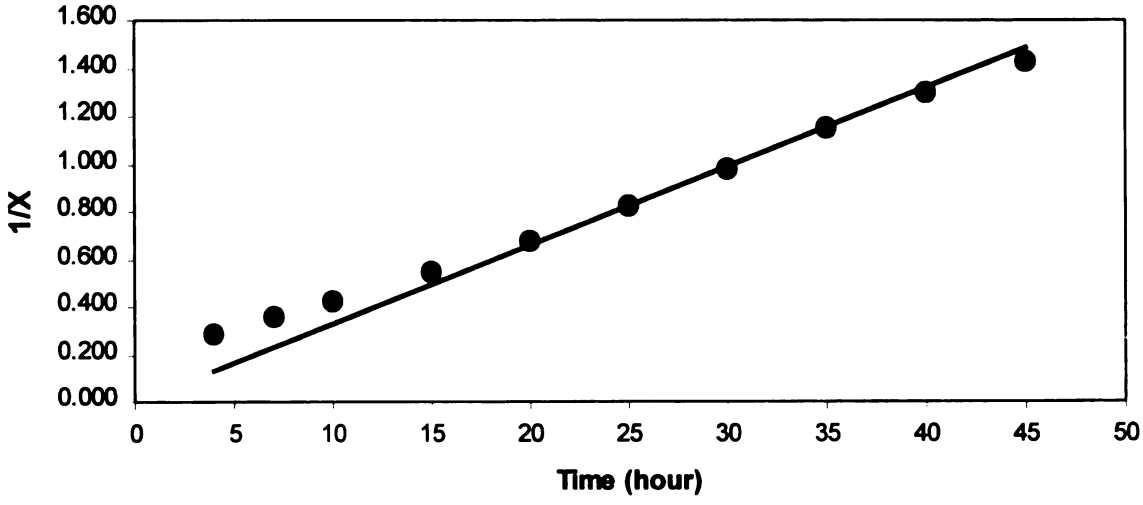

Figure 9 The "1/X versus time" plot of 0.675mil non-clay polyimide film at ethyl acetate vapor activity a = 0.68 and T = 23 °C. (Slope = 0.0329, $R^2 = 0.965$, $D = 6.6 \times 10^{-16}$ m^2/sec)

H. Calculation of solubility coefficient

The solubility coefficient (S) is usually determined by observing the change in weight of a polymer sample during a sorption process. Such a process can involve the absorption or desorption of low molecular weight moieties by the polymer sample.

To relate the concentration of the penetrant (C) in the polymer to the penetrant concentration in the gas or vapor phase in equilibrium with the polymer, Henry's law is assumed:

$$C = S\ p \qquad (3)$$

where p is the partial pressure of the penetrant in the gas phase. The partial pressure of the penetrant is further related to the penetrant concentration in the gas phase through the ideal gas law.

As discussed in the Results and Discussion section (see page 65), the ethyl acetate sorption isotherm, assumes a dual-mode sorption model of ordinary dissolution and adsorption into the microvoids ("hole") for vapor sorption in the glassy amorphous polyimides. The sorption isotherm for this polymer was accurately described by the dual-mode sorption model (Equation 8).

$$C = C_H + C_D = \frac{C'_H bp}{1 + bp} + k_D p \qquad (8)$$

From the isotherm, the changes in the vapor partial pressure are not consistent with the changes in the solubility values. If the Henry's law component contributes only a portion of the ethyl acetate uptake described by the sorption model, the solubility coefficient (S) will be given by:

$$S = \frac{\partial C}{\partial p} = \frac{C_H' b}{(1 + bp)^2} + k_D \qquad (26)$$

Solving Equation (26) thus gives the tangent value of the sorption isotherm at each vapor partial pressure. The S values determined by this procedure, show how the vapor partial pressure affects the solubility values.

I. Calculation of parameters of dual-mode sorption methods

Calculation of the sorption parameters C'_H, k_D, b from the sorption isotherm data was carried out as following:

$$C = C_H + k_D p \qquad (27)$$

This form of equation (27) indicates that a quantitative separation of the sorption contributions is possible at high partial pressures, assuming the dual mode sorption model adequately describes the data. Since the expression is in a linear form, a plot of C as a function of p give a slope equal to k_D and the y-intercept equal to C'_H. After k_D has been determined from the slope of the best straight lines through the high partial pressure data, the 'hole' contribution, C_H, for each vapor pressure can be determined by subtracting $k_D p$ from C.

$$C_H = C - k_D p \qquad (28)$$

Also the expression for C_H can be rearranged to the form;

$$\frac{p}{C_H} = \frac{1}{C'_H b} + \frac{p}{C'_H} \qquad (29)$$

Then the Langmuir plot, p/C_H versus p, should yield a straight line of slope $1/C'_H$ and intercept at (p = 0) of $1/C'_Hb$. This procedure, as in most procedures involving curve fitting of the data, is of a trial and error nature and it is continued until the best (least mean-squares) fit of the data on the Langmuir plot is achieved. This procedure is illustrated in Figure 10 & 11.

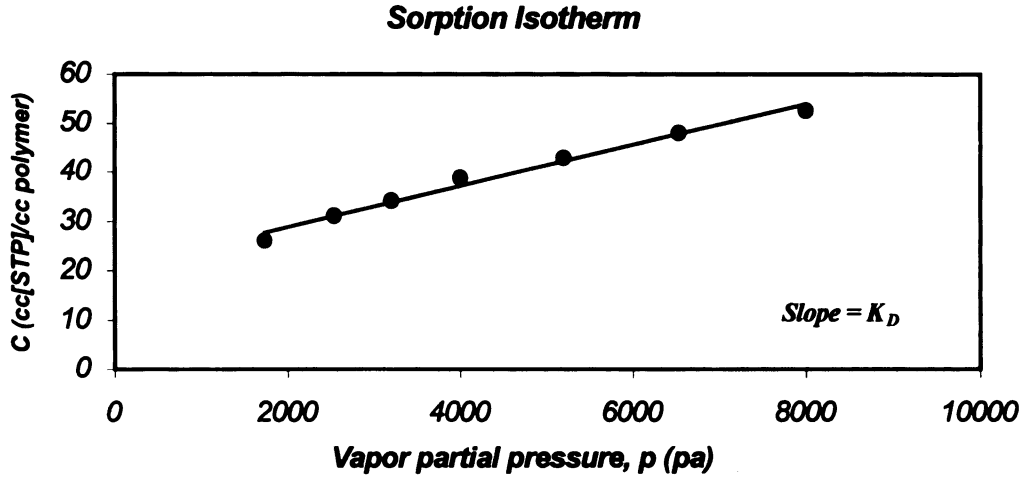

Figure 10. Determining the Henry's law constant by dual-mode sorption model

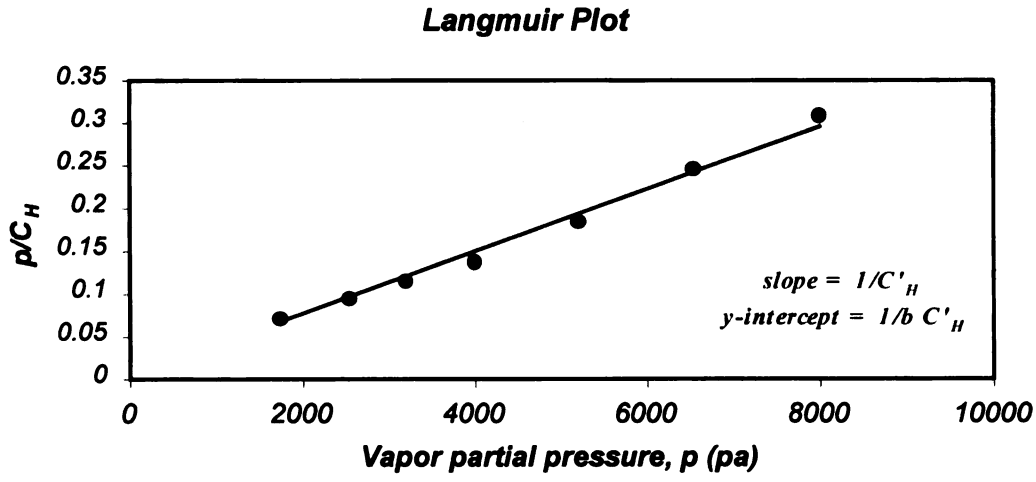

Figure 11. Determining parameters by Langmuir Plot

Results and Discussion

Sorption Properties

1. Equilibrium Solubility for Ethyl Acetate Organic Vapor

The solubility at equilibrium of ethyl acetate in a polyimide film was obtained from the weight gain of the sample at long sorption times, where weight gain is determined at steady state. A representative plot of M_t / M_{ss}, as a function of time, for the sorption of ethyl acetate by the non-clay polyimide film, is presented in Figure 12. The theoretical sorption curve obtained by solution of Equation 22 is superimposed for comparison.

$$\frac{M_t}{M_\infty} = 1 - \sum_{n=0}^{\infty} \frac{8}{(2n+1)^2 \pi^2} \exp\left[\frac{-D\pi^2(2n+1)^2 t}{l^2}\right] \qquad (22)$$

The sorption behavior of clay-loading polyimide film (2.5 v/v%) is illustrated in Figure 13 and is representative of the sorption profile curves obtained for the respective clay/polyimide composites studied. The theoretical sorption curve for the clay/polyimide film is also presented in Figure 13 for comparison.

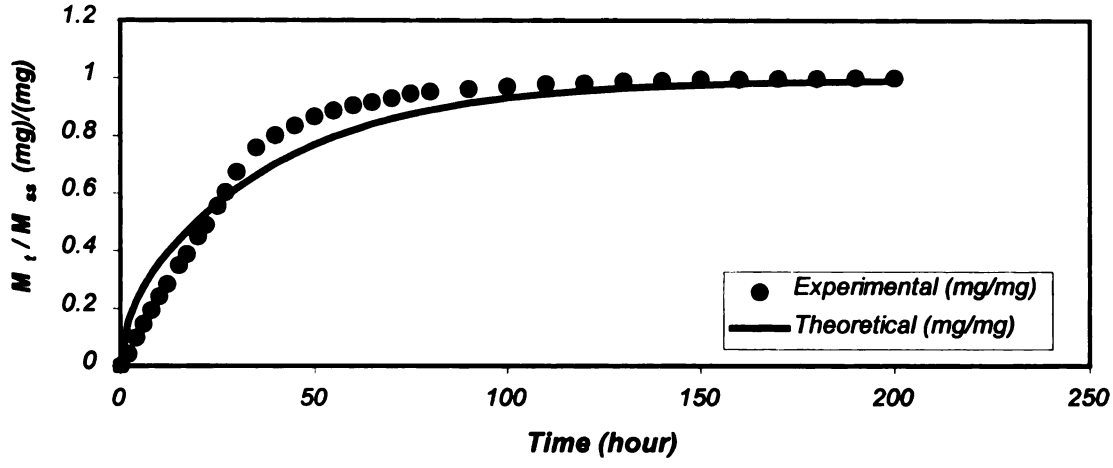

Figure 12 A representation plot of M_t / M_{ss} as a function of time, for the sorption of ethyl acetate by the non-clay polyimide film. ($a_v = 0.68$)

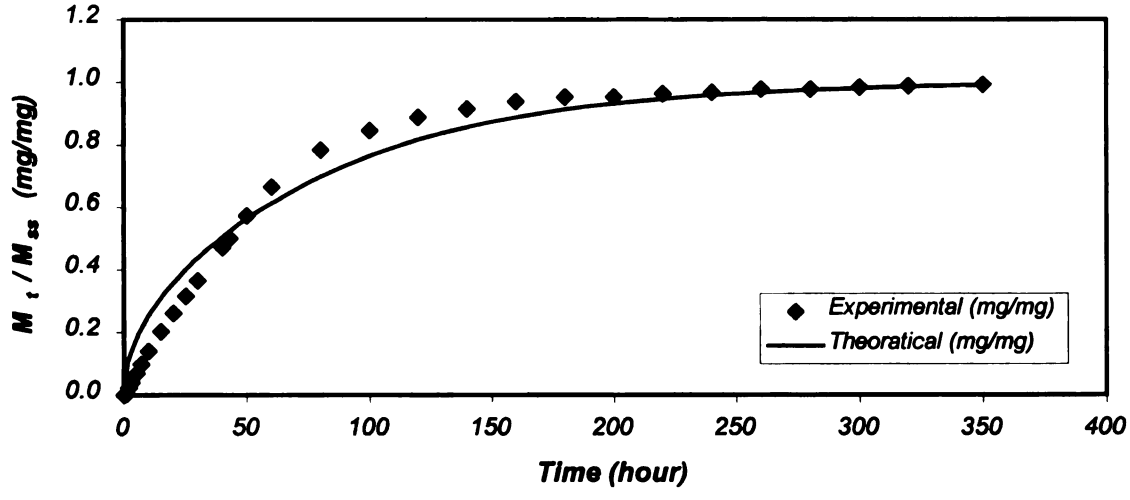

Figure 13 A representation plot of M_t / M_{ss} as a function of time, for the sorption of ethyl acetate by the 2.5 v% polyimide-clay film. ($a_v = 0.68$)

It can be seen that the theoretical curve lacks a good fit to the experimental data, and as shown, the initial portion of the experimental data is approximated by a straight line. The lack of good agreement between the experimental and calculated sorption data can be explained by the fact that a calculated D value can not accurately account for the whole sorption kinetics in the limited range of diffusion coefficient variations. The equilibrium solubility values (C) and the time values to equilibrium (t_{ss}) determined for ethyl acetate in non-clay and clay loaded polyimide composites ranging from 1.25 % to 5% (v/v) are summarized in Table 3 and Table 4, respectively. As shown, while the sorption time to equilibrium varied dramatically as a function of clay loading, the equilibrium solubility of ethyl acetate in the unfilled polyimide and clay/polyimide composite membranes was relatively constant at the respective vapor activity levels studied. It can be concluded that the polymer matrix and clay filler have similar organic vapor absorption properties, and the clay has neither a synergetic or antagonistic effect on the solubility of organic vapor in the polyimide matrix.

Table 3 Vapor activity dependence of solubility values in polyimide-clay nanocomposites (23 ± 1 °C)

Ethyl acetate vapor activity	0 v% clay [a] Polyimide film (mg/mg polymer)	1.25 v% clay Polyimide film (mg/mg polymer)	2.50 v% clay Polyimide film (mg/mg polymer)	5.0 v% clay Polyimide film (mg/mg polymer)
0.68	**0.141 ±0.002**	**0.130**	**0.124**	**0.116**
0.55	**0.126 ±0.004**	**0.120**	**0.115**	
0.44	**0.112 ±0.002**	**0.108**	**0.104**	
0.34	**0.101 ±0.001**	**0.096**		
0.27	**0.091 ±0.002**	**0.082**		
0.21	**0.082 ±0.002**			
0.15	**0.067 ±0.002**			

[a] Solubility values are the average of at least two sorption tests.

Table 4 Variation in normalized sorption time (t_{ss}) to equilibrium in polyimide-clay nanocomposites (23 ± 1 °C, 1mil film thickness)

Ethyl acetate vapor activity	0 v% clay Polyimide film (hours)	1.25 v% clay Polyimide film (hours)	2.50 v% clay Polyimide film (hours)	5.0 v% clay Polyimide film (hours)
0.68	**188**	**255**	**313**	**509**
0.55	**369**	**457**	**788**	
0.44	**569**	**787**	**1089**	
0.34	**700**	**1667**		
0.27	**957**	**2034**		
0.21	**1108**			
0.15	**1358**			

* The time value to equilibrium (t_{ss}) is calculated by the time value which is equal to 6 times of $t_{1/2}$ (half-sorption time value).

The sorption capacity of the organo-clay inclusion was also determined and compared to the solubility of ethyl acetate in the non-clay loading polyimide membrane. The results are summarized in Table 5. As shown, the clay filler and the polymer matrix exhibit comparable sorption properties for ethyl acetate vapor.

Table 5 Equilibrium solubility values (mg/mg sorbant) of clay powder and unfilled polyimide film.

Ethyl acetate vapor activity	0.68	0.44	0.27
Clay powder	**0.131**	**0.082**	**0.055**
Original polyimide	**0.141**	**0.112**	**0.091**

With regard to the equilibrium solubility determined for the respective clay/polyimide hybrid membrane, it can be assumed that the solubility value is the sum of the polymer equilibrium solubility value and the clay inclusion solubility value.

Equation 30 can therefore be used to estimate the solubility values of the clay loading polyimide nanocomposites.

$$C_{est} = (1 - M_f) C_p + M_f C_c \qquad (30)$$

where M_f is the weight fraction of the clay inclusion in the composite. In this case, the weight fraction of the clay is equal to two times the volume fraction of the clay (v_f). C_p and C_c are the solubility values of the non-clay polymer and the clay powder itself, respectively. Estimated values for the equilibrium solubility of ethyl acetate in the 1.25% (v/v) clay/polyimide hybrid are summarized in Table 6. The determined solubility values are also listed for comparison. As shown, good agreement was obtained between the experimental and calculated solubility values. This is also shown graphically in Figure 14, when calculated and experimental solubility values are compared for the 1.25 v/v% clay/polyimide composite at selected ethyl acetate activity levels.

Table 6 Comparison of experimental and calculated absorption properties of a polyimide clay hybrid as a function of ethyl acetate vapor activity

Vapor activity / **Solubility** (wt/wt sorbant)		a = 0.68	a = 0.44	a = 0.27
C_p	Polyimide	**0.141**	**0.112**	**0.091**
C_c	Clay powder	0.131	0.082	0.055
C_{exp}	1.25 v% polyimide-clay hybrid	**0.130**	**0.108**	**0.082**
C_{est}	1.25 v% clay + 98.75 v% polyimide	**0.141**	**0.110**	**0.090**

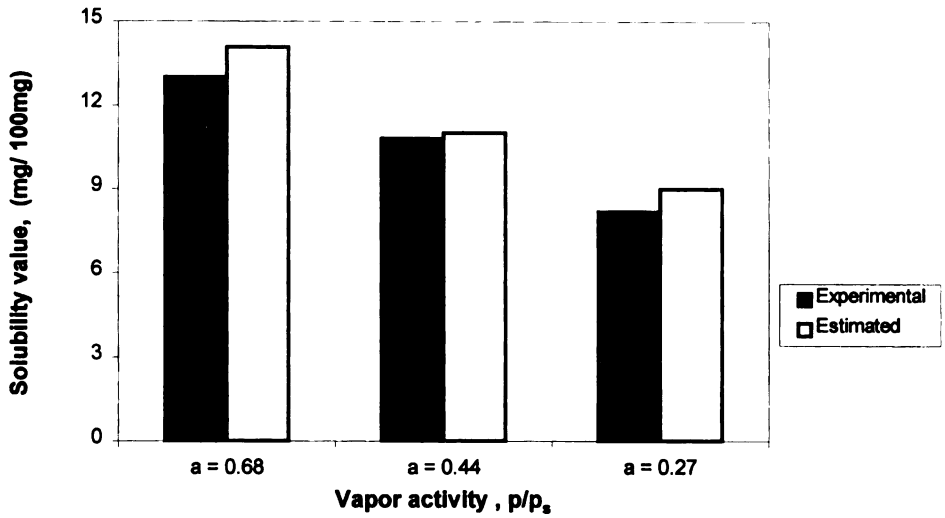

Figure 14 Solubility values comparison for the 1.25 v/v% clay-loading polyimide composite, between the experimental and calculated values.

2. Solubility coefficient

The equilibrium solubility coefficient values (S) determined for the respective polyimide-clay nanocomposites membranes are summarized in Table 7. The S values reported were determined by the tangent methods, as discussed in the Materials and Methods section. Typical plots of the calculated solubility coefficient (S) as a function of ethyl acetate vapor pressure for the non-clay loading and clay-loading (1.25 % v/v) polyimide membrane are presented in Figures 15 and 16, respectively. As shown, with increasing vapor activity, the solubility coefficient (S) decreases and approaches a constant at high activity levels (i.e. $a_v > 0.5$). The Henry's law constant, k_D, would be the lower limit of the solubility coefficient.

Table 7 The calculated solubility coefficients S (cc [STP]/cc . pa^{-1}) for the non-clay and 1.25 % v/v polyimide clay nanocomposites.

Vapor activity	Vapor partial pressure (pa)	Solubility coefficient (0% v/v polyimide films)	Solubility coefficient (1.25 % v/v polyimide films)
0.15	1694	0.00456	0.00438
0.21	2458	0.00440	0.00424
0.27	3205	0.00434	0.00419
0.34	4065	0.00431	0.00417
0.44	5111	0.00429	0.00415
0.55	6326	0.00427	0.00414
0.68	7894	0.00426	0.00413

As shown, with increasing vapor activity, changes in the solubility coefficient between the hybrid and polyimide matrix are almost imperceptible, over the whole range of vapor activities studied. Clay did not appear to influence the sorption of ethyl acetate vapor by the polyimide film, at the concentrations evaluated. For the respective nanocomposite films, the solubility coefficients were similar to the solubility coefficient

values obtained for the non-clay polyimide films, at comparable vapor activity levels. As shown in Table 7, and from Figures 15 and 16, it was found that the solubility coefficient values were independent of vapor activity, at vapor activity values great than 0.5. For the polyimide-clay nanocomposite, the clay appears to have little effect on the solubility of ethyl acetate in the polyimide film, while significantly changing the inherent mobility of ethyl acetate vapor within the polymer bulk phase. Okamoto et al. (1992) observed similar behavior for water sorption by the same type of polyimide film, where the solubility coefficient increased at low water vapor activities and leveled off at medium and high water activities.

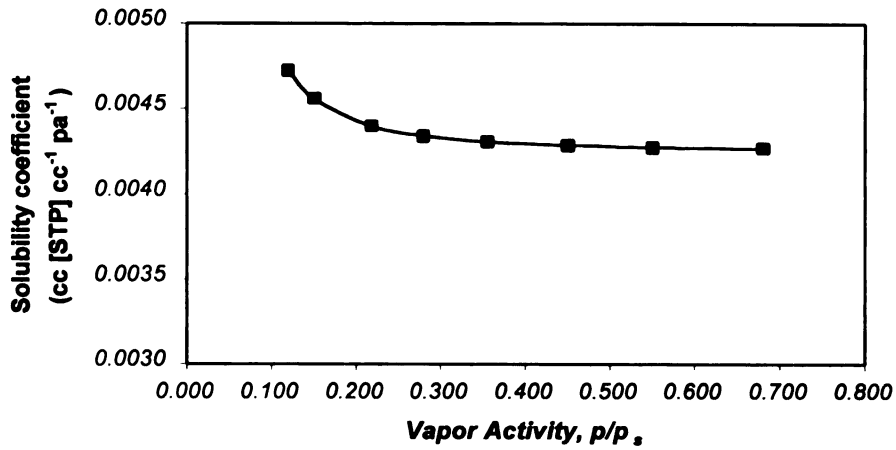

Figure 15 Solubility coefficients of non-clay polyimide films

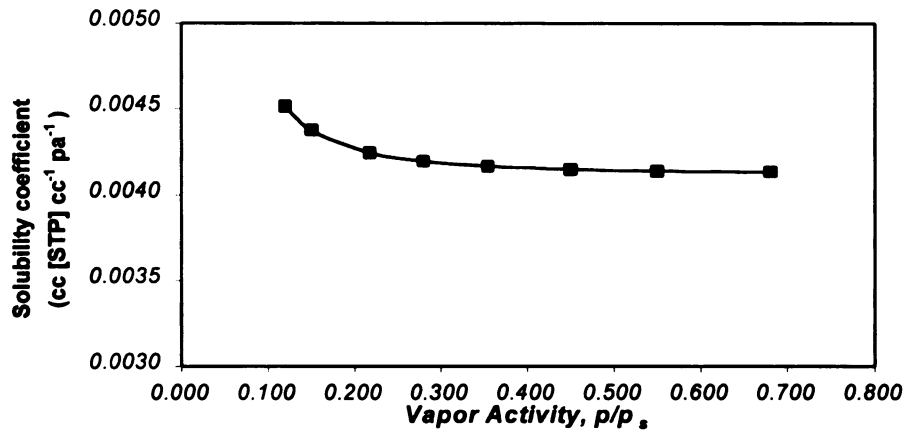

Figure 16 Solubility coefficients of 1.25 v/v % clay/polyimide films.

3. Dual mode sorption parameters

The sorption isotherms obtained for the non-clay polyimide and 1.25 v/v % clay/polyimide nanocomposite are presented in Figures 17 and 18, respectively, with the calculated sorption isotherm curve obtained from Equation 8 superimposed for comparison. As shown, the sorption isotherm obtained for this polymer is concave to the activity axis at low activity and linear at higher activity levels and was accurately described by Equation 8, the dual-mode sorption model. Okamoto et al. (1992) found that for water sorption by the same type of polyimide film, the sorption isotherms of water vapor in polyimide films were in good agreement with the dual-mode sorption model. Okamoto et al. (1992) proposed that the large values of both k_D and b and the small values of C'_H are characteristic of water vapor sorption in the polyimide films, as compared with the respective constants describing CO_2 sorption. The large values of both k_D and b are suggestive of interaction between imide groups and water molecules. Large values of both k_D and b and a small value of C'_H cause appreciable deviation from the Henry's law isotherm, in the low vapor activity region.

$$C = k_D p + \frac{C'_H bp}{1 + bp} \qquad (8)$$

The dual mode sorption parameters for the ethyl acetate vapor/polyimide film system are summarized in Table 8. The constants for water vapor sorption by the same type of polyimide film, as reported by Okamoto et al. (1992), are also given for comparison. According to the dual mode sorption model, the total quantity of penetrant

sorbed (C) is comprised of the Henry's law component (C_D) and the "hole" filling components (C_H). The Henry's law solubility (C_D) and the Langmiur solubility (C_H) values are plotted as a function of vapor pressure for the ethyl acetate/polyimide system in Figures 19 and 20, respectively. As shown in Figure 20, the "hole" filling component of the polymer matrix is saturated by organic vapor, when the vapor pressure exceeded 1600 pa. The small values of k_D (Henry's law solubility constant) and the large values of C'_H (Langmuir capacity constant) are characteristic of organic vapor sorption in the polyimide films, as compared to water vapor sorption.

Table 8 Dual-Mode Sorption Parameters for Polyimide film

	k_D *cc(STP)/cc • pa*	*b* pa^{-1}	C'_H *[cc(STP)/cc]*
Ethyl acetate vapor 23 °C (Non-clay)	0.00425	0.0218	20.5
Ethyl acetate vapor 23 °C (1.25 v% clay)	0.00412	0.0252	19.6
Water vapor 50 °C [a] (Non-clay)	0.00630	0.0022	6.0

[a] Okamoto K., 1992. " Sorption and Diffusion of Water Vapor in Polyimide Films". *Journal of Polymer Science: Polymer Physics Edition* **30**: 1223.

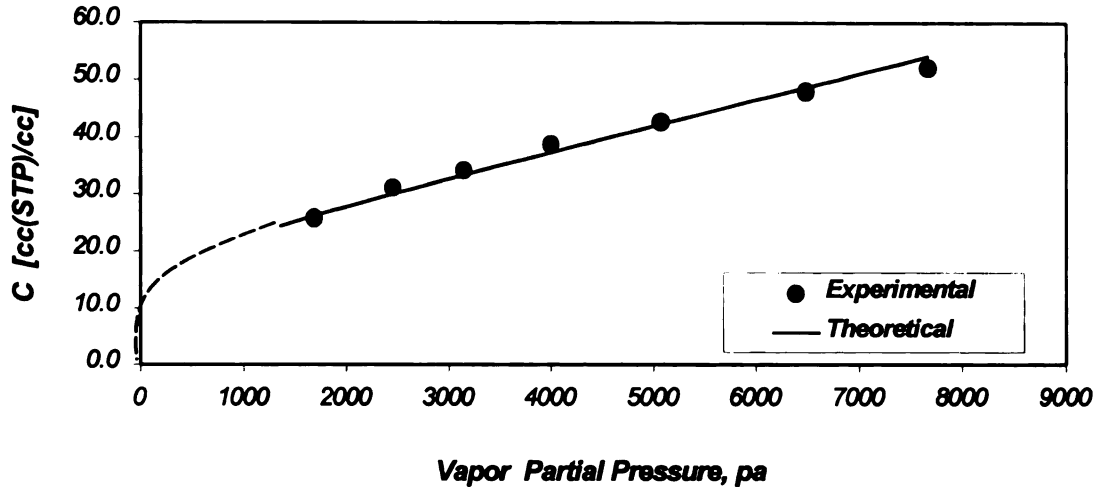

Figure 17. Typical sorption isotherm of ethyl acetate in non-clay polyimide films at 23°C

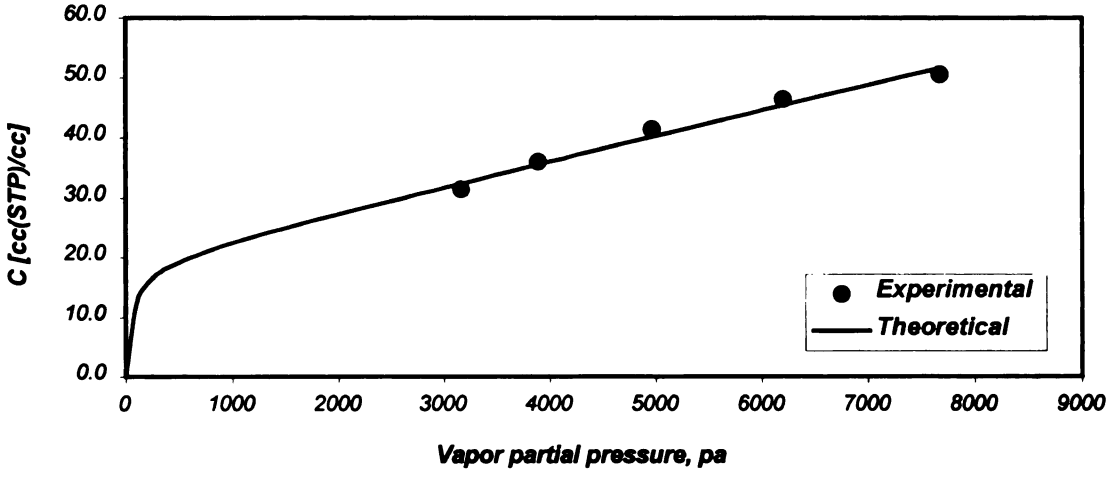

Figure 18. Typical sorption isotherm of ethyl acetate in 1.25 v/v % clay/polyimide films at 23°C

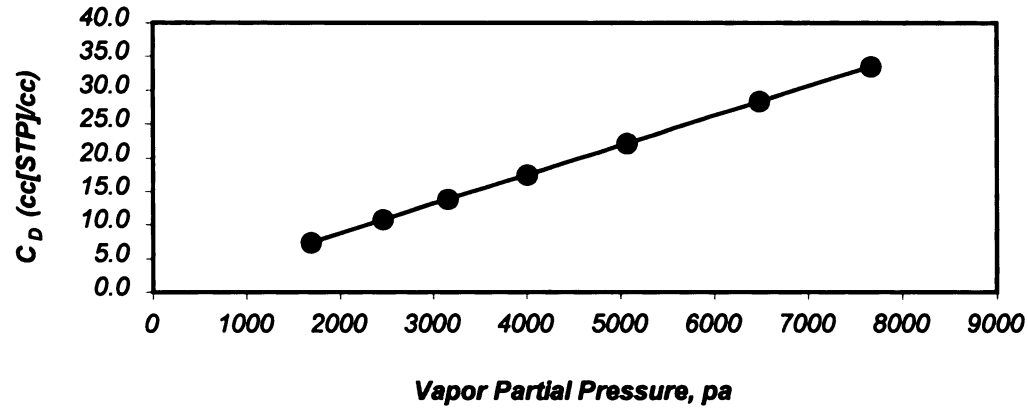

Figure 19. Concentration ($C_D = K_D \bullet p$) by Henry's Law is a function of the vapor pressure.

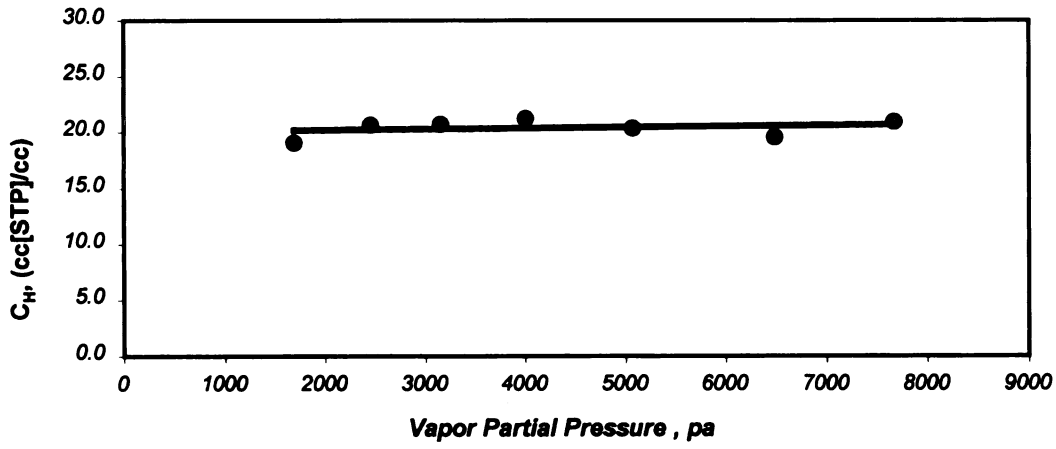

Figure 20. Langmuir solubility ($C_H = C - C_D$) is not a function of the vapor pressure at a relatively high vapor partial pressure.

Diffusion Properties

For the sorption of the ethyl acetate by the non-clay polyimide films and clay-loading films, the experimental sorption curve was found to deviate from the theoretical data. These findings would indicate that the sorption process might follow non-Fickian behavior. Thus, the diffusion coefficient values were determined by the application of the curve fitting methods described in the Materials and Methods section (see Page 44 - 51). Tables 9 & 10 summarize the diffusion coefficient values determined by the respective curve fitting methods, over a range of vapor activity levels. As shown, in Tables 9 and 10, the calculated diffusion coefficients appear to be similar, for the respective methods. In the present study, the Least Squares Method was used to calculate the diffusion coefficients. For validating the diffusion coefficient variance, the Least Squares Method provides an integration procedure which includes the entire sorption data. Also, the diffusion coefficients would be consistent with the data obtained from earlier studies, which used the same least square method (Barr, 1997).

Table 9 Diffusion coefficient values (m^2/s) for non-clay polyimide films, determined as a function of vapor activity.

Vapor Activity (a_v)	Diffusion Coefficients By Gauss-Newton method	Diffusion Coefficients By Half sorption time method	Diffusion Coefficients By Least Squares method
0.15	0.347×10^{-16}	0.388×10^{-16}	0.401×10^{-16}
0.21	0.460×10^{-16}	0.476×10^{-16}	0.537×10^{-16}
0.27	0.479×10^{-16}	0.551×10^{-16}	0.608×10^{-16}
0.34	0.700×10^{-16}	0.754×10^{-16}	0.875×10^{-16}
0.44	0.884×10^{-16}	1.036×10^{-16}	1.290×10^{-16}
0.55	1.380×10^{-16}	1.429×10^{-16}	1.725×10^{-16}
0.68	2.780×10^{-16}	2.808×10^{-16}	3.290×10^{-16}

Table 10 Diffusion coefficient values (m^2/s) for clay-loading polyimide films, determined as a function of clay loading and vapor activity.

Clay Loading	Vapor activity (a_v)	Diffusion coefficients By Gauss-Newton method	Diffusion coefficients By Half sorption time method	Diffusion coefficients By Least Squares method
1.25v%	0.27	0.215×10^{-16}	0.259×10^{-16}	0.292×10^{-16}
	0.34	0.255×10^{-16}	0.305×10^{-16}	0.351×10^{-16}
	0.44	0.515×10^{-16}	0.669×10^{-16}	0.715×10^{-16}
	0.55	1.025×10^{-16}	1.153×10^{-16}	1.280×10^{-16}
	0.68	1.995×10^{-16}	2.066×10^{-16}	2.290×10^{-16}
2.5 v%	0.44	0.451×10^{-16}	0.484×10^{-16}	0.555×10^{-16}
	0.55	0.611×10^{-16}	0.669×10^{-16}	0.745×10^{-16}
	0.68	1.555×10^{-16}	1.684×10^{-16}	1.903×10^{-16}
5.0 v%	0.68	0.885×10^{-16}	1.035×10^{-16}	1.160×10^{-16}

1. Effect of Ethyl Acetate Vapor Activity

Diffusion coefficient values obtained from the gravimetric experiments are presented in Table 11. For better illustration, the results obtained for the non-clay loading polyimides and the 1.25 v/v % polyimide/clay nanocomposites films are presented graphically in Figures 21 and 22, respectively. As shown, in Table 11 and Figures 21 & 22, for the non-clay loading polyimide and the 1.25 v/v % clay composites, diffusion coefficient values increased with an increase in vapor activity of ethyl acetate, indicating a concentration dependency of the diffusion coefficient. Okamoto et al. (1992) found that for water sorption by a similar polyimide film, the diffusion coefficient increases at low water vapor activities and leveled off at medium and high water activities.

Integral sorption from zero pressure was investigated. Figure 23 shows typical normalized sorption curves of non-clay polyimide nanocomposites. M_t and M_{ss} refer to the mass sorbed at time t and the mass sorbed at steady state, respectively. Plots of M_t / M_{ss} versus time initially were linear. As shown, equilibrium sorption was achieved within 100 hours at $a_v = 0.68$ and 500 hours at $a_v = 0.27$, judging from the diffusion coefficient. At low vapor activity, the approach to equilibrium is extremely protracted, indicating the presence of a slow, minor component of sorption in addition to the normal, major mode of sorbate uptake.

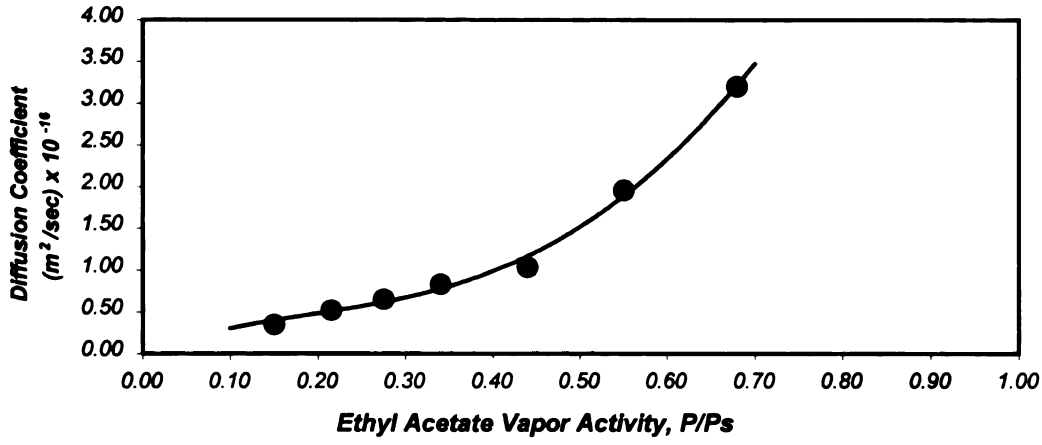

Figure 21 Diffusion Coefficients of non-clay polyimide film versus organic vapor activity.

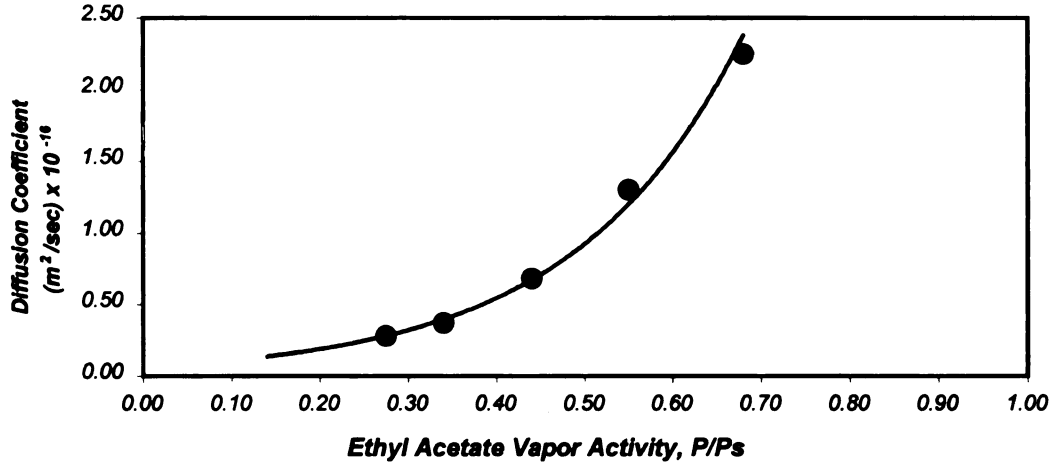

Figure 22 Diffusion Coefficients of 1.25 v% polyimide-clay nanocomposite films versus organic vapor activity

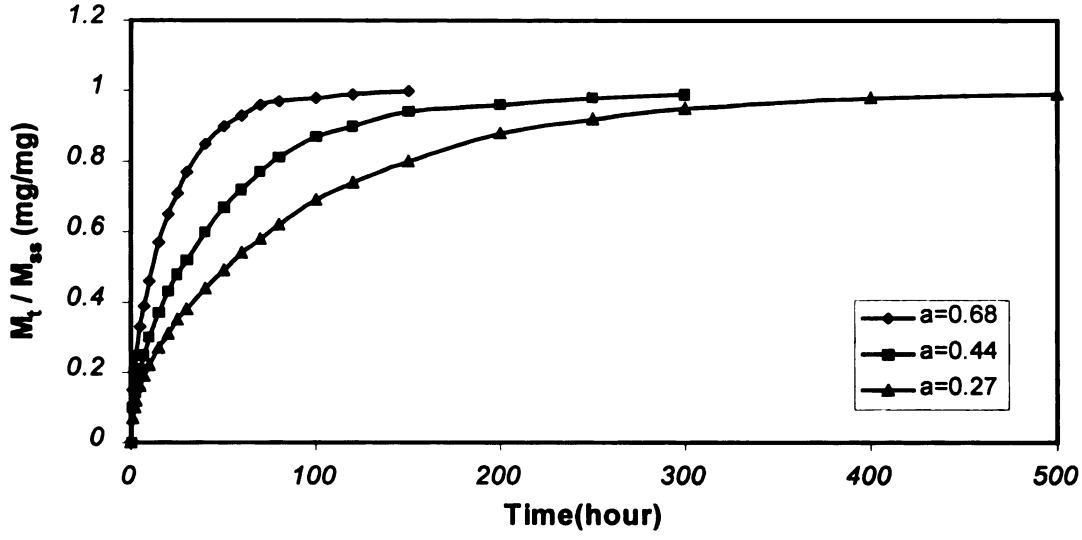

Figure 23 Variation in normalized sorption of ethyl acetate in non-clay polyimide film with time after introduction of vapor at 23 °C. Diffusion coefficients are 3.2, 1.2, and 0.6 (x 10^{-16} m^2/s), respectively.

Table 11 Vapor activity dependence of diffusion coefficient values (x 10^{-16} m^2/s) in polyimide-clay nanocomposites.

Vapor activity	Clay loading 0 v/v% [a]	Clay loading 1.25 v/v%	Clay loading 2.50 v/v%	Clay loading 5.00 v/v%
0.68	3.25 ± 0.04	2.29	1.90	1.16
0.55	1.69 ± 0.04	1.28	0.75	
0.44	1.13 ± 0.14	0.72	0.56	
0.34	0.89 ± 0.05	0.35		
0.27	0.65 ± 0.06	0.29		
0.21	0.48 ± 0.06			
0.15	0.36 ± 0.06			

a. Diffusion coefficient values are the average of at least two sorption tests.

The data obtained showed a significant increase in the diffusion coefficient with an increase in vapor activity for the non-clay loading polyimide and the 1.25 v/v % clay/polyimide nanocomposite. Such dependence is well known for a number of polymer-permeant systems, for which an exponential relationship was proposed (Crank, 1951). The permeation data through a film can be accounted for by a diffusion coefficient, which increases exponentially with an increase in the local solute content in the polymer film, as described by Equation (31):

$$D = D^* \exp(\gamma C) \qquad (31)$$

Where D^* is the limiting diffusion coefficient and γ is a coefficient that can be interpreted as characterizing the ability of a penetrant to 'plasticize' a polymer, i.e. to increase the polymer segmental chain mobility.

Schematically, the polymer structure is loosened as penetrant molecules are inserted between polymer segments, and more free volume is available for penetrant diffusion. The molecular origin of the exponential dependence of the diffusivity on both penetrant concentration and polymer free volume can be found in the free-volume theory (Neogi, 1996) (Meares, 1993). Figures 21 and 22 indicate that the diffusion coefficient for ethyl acetate increases exponentially with its local concentration in the polymer membranes.

On the other hand, it should be noted that the observed increase in the diffusion coefficient, with increased solute content in the polymer, must not lead to a value larger than that of the solute self-diffusion coefficient. In fact, being limited by the extent of penetrant sorption, the diffusion coefficients increase less than tenfold, over a vapor activity range from the vacuum state to saturated state. In the case of the polyimide-clay nanocomposite of 1.25 v% clay loading, the diffusion coefficients increase about six-fold, when vapor activity increased from 0.3 to 0.7.

The exponential relationship found between the diffusion coefficient and vapor activity for the polymer film is consistent with the results obtained by Perrin (1996) on the water/polyvinyl alcohol (PVA) system, but shows a lack of agreement with the results reported by Okamoto et al. (1992) on the water/Polyimide system and Gu (1997) on the ethyl acetate/Polyimide system. Gu (1997) reported that ethyl acetate vapor concentration did not significantly affect the permeability coefficient values for the same polyimide films, over a vapor pressure range between 1700 to 3200 Pa. The results of the permeability studies reported by Gu are summarized in Table 12. The diffusion coefficient values determined by Gu (1997) and the values obtained in the present study are summarized in Table 13. The lack of agreement between the diffusion coefficient values reported by Gu and those obtained in the present sorption studies is not fully understood and a clear explanation for the discrepancy between these two cases can not be provided. The present studies suggest that the behavior of the diffusion coefficients is

the result of the effect of local chain organization, clay dispersion, polymer matrix morphology and the distribution of clay domains.

Table 12. Effect of ethyl acetate vapor pressure on the permeability of Clay/polyimide composite films at 23 °C in the Literature (Gu, 1997).

Vapor activity (a_v)	Ethyl acetate partial pressure (Pa)	Permeability Coefficient (Kg m/(m^2 sec pa))	
		0 v/v % Clay	2.5 v/v% Clay
0.27	3200 (24.36 mmHg)	1.24×10^{-18}	0.188×10^{-18}
0.15	1700 (12.87 mmHg)	1.14×10^{-18}	0.127×10^{-18}

Table 13. Comparison of the diffusion coefficient values of Non-clay polyimide composite films/Ethyl acetate at 23 °C between the Literature (Gu, 1997) and this study.

Vapor activity (a_v)	Ethyl acetate partial pressure (Pa)	Diffusion Coefficient (m^2 /sec)	
		Literature	This Study
0.27	3200 (24.36 mmHg)	$(3.1 \pm 0.2) \times 10^{-14}$	$(6.5 \pm 0.6) \times 10^{-17}$
0.15	1700 (12.87 mmHg)	$(5.7 \pm 1.3) \times 10^{-14}$	$(3.6 \pm 0.6) \times 10^{-17}$

2. Effect of Clay-Loading on Polyimide-clay Nanocomposites

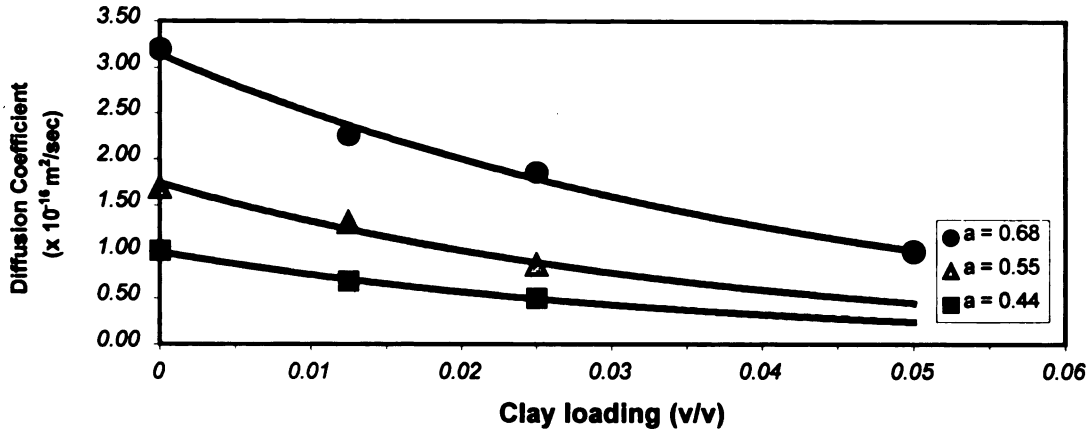

Figure 24 Clay-loading Dependence of diffusion coefficients in Polyimide-clay Nanocomposites

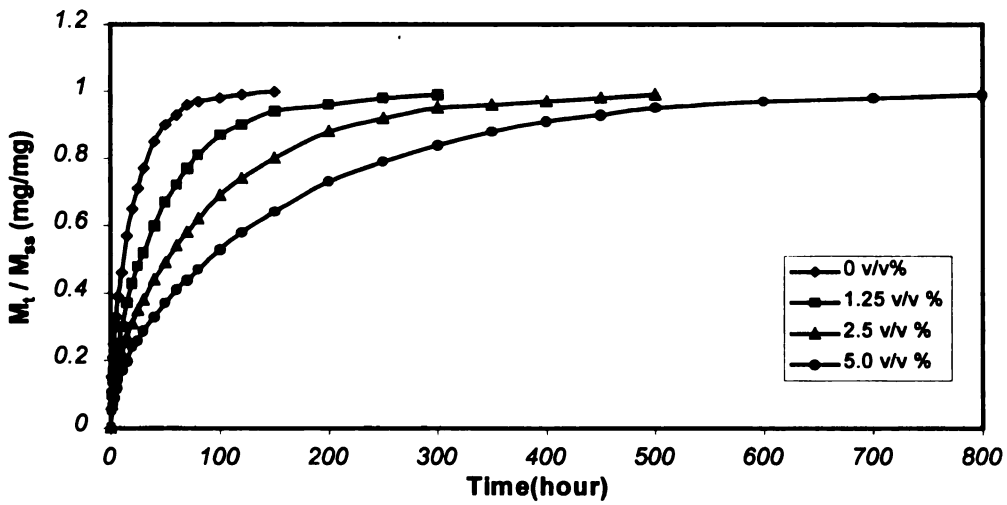

Figure 25 Variation in clay-loading dependency of normalized sorption of ethyl acetate (a = 0.68) in polyimide/clay films with time after introduction of vapor at 23 °C. Diffusion coefficients are 3.3, 2.2, 1.9, and 1.1 (x 10^{-16} m^2/s), respectively.

Figure 24 shows the variation of the diffusion coefficient as a function of the clay loading level. Also, Figure 25 presents typical normalized sorption curves, as a function of clay loading. As shown in Figure 25, at high clay loading, the approach to equilibrium sorption levels is extremely protracted, indicating the presence of a longer diffusion path through the film. This is illustrated in Figure 24, which shows that, with an increase in clay loading, the diffusion coefficient decreased dramatically. The function of the clay can be interpreted as characterizing the ability to 'modify' the polymer, i.e. to increase the diffusion path of a diffusing gas through the polymer matrix. For a gas-impermeable clay, the diffusion coefficient values may only be determined by the aspect ratio (L/W) of the clay inclusion and the clay loading v_f.

These results also show that the effect of clay loading and organic vapor activity are independent. As a result, the degree of improvement of the barrier properties of polyimide/clay nanocomposites depends on the clay inclusion. It appears that the clay restricts the permeant mobility by decreasing the diffusion coefficient. The decrease in the diffusion coefficient can be explained by an increase in the tortuosity of the diffusion path and also by a restriction of the mobility of the polymer segments blocked in the impermeable clays. The greater the level of clay loading, the lower the effectiveness of penetrant diffusivity, at the same penetrant concentration. However, no model is available to account for the above effects.

Such dependence found between the diffusion coefficient and the volume fraction of clay inclusion in the polymer film is consistent with the results obtained by Gu (1997) (See Table 12), who reported that the clay-loading level dramatically affected the permeability coefficient values for the same polyimide films. The results of the sorption and permeability studies show that the mineral clay inclusion dramatically improved the barrier properties of intercalated and exfoliated polyimide-clay nanocomposite films.

3. Aspect Ratio and Tortuosity

As shown by transmission electron microscopy (TEM), for the clay/polyimide composites, montmorillonite is disposed parallel to the film surface. (Lan, 1994) In this case, the total path of diffusing gases is increased. If montmorillonite plates of length L and width W, are dispersed parallel within the polymer matrix, the tortuosity factor τ, which can be directly calculated by the aspect ratio (L/W), is the main factor in controlling the diffusivity of the vapor through the polymer matrix (Nielsen, 1967).

As previously discussed, (see page 56 - 58), the clay loading level doesn't appear to effect the solubility values and the respective solubility coefficients, where S_c and S_p (S_c and S_p are the solubility coefficient values for the composite and polymer matrix, respectively) are equivalent. In Equation (18), the relative permeability data can therefore be replaced by the relative diffusion coefficient data. Therefore, the relative diffusion coefficient ratio (D_c / D_p), where D_c and D_p are the diffusion coefficients for the composite and polymer matrix, respectively, is given by Equation (32):

$$\frac{D_c}{D_p} \cong \frac{P_c}{P_p} = \frac{D_c S_c}{D_p S_p} = \frac{1}{1 + (L / 2W) v_f} \qquad (32)$$

where v_f represents the volume fraction of clay, and the aspect ratio (L/W) can be estimated from the experimental diffusion coefficient data.

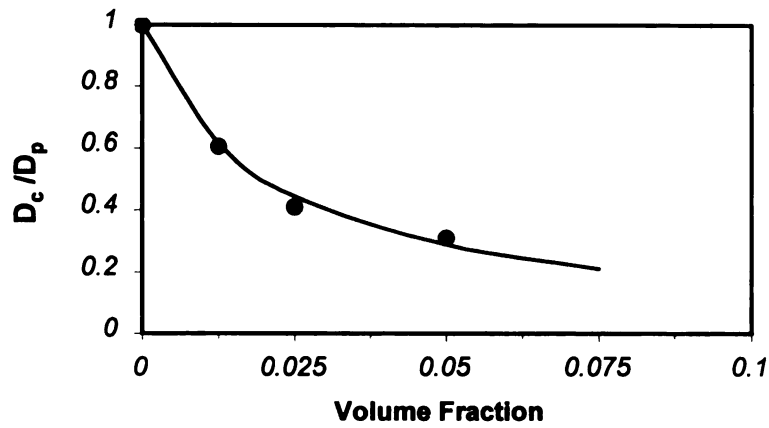

Figure 26 Relative diffusion coefficient value of polyimide-clay nanocomposite at ethyl acetate vapor activity = 0.68 @23 °C 0%RH.

Based on this expression, an effective aspect ratio was estimated from the diffusion coefficient data (D_c/D_p). Figure 26 illustrates the results obtained by application of Equation 44 to the experimental data. The solid curve represents the best fit of the calculated values from Equation 45 to the experimental data. The best-fit curve yields an effective clay aspect ratio of approximately 100 from the ethyl acetate sorption studies. Table 14 summarizes the estimated aspect ratio values obtained from the permeability data reported in the literature for similar clay/polyimide composites. The aspect ratio determined in the present study fell within the range reported in the literature. It should be noted that the films used in this study were the same films employed by Gu (1997). Also, it is further assumed that the clay texture in the nanocomposite films evaluated in the present study is similar to that obtained by Lan (1994) and Yano (1993), since the

methodologies employed in the respective studies in preparing the nanocomposite films were similar.

Table 14 Comparison of the estimated aspect ratio with the literature data.

Penetrant (23 °C)	Source	Estimated Aspect Ratio
Ethyl Acetate	**This study**	**100**
Water	Gu, 1997	132
CO_2	Gu, 1997	83
O_2	Gu, 1997	87
CO_2	Lan, 1994	192
Water	Yano, 1993	200

It should be pointed out that the diffusion path model described is based on the assumption that the impermeable clay layers are perfectly oriented and evenly spaced within the matrix of the polymer. However, this situation is not likely to be realized in actual composite structures (Messersmith 1995).

As described above, a low loading level (i.e. 5% wt/wt) of clay improves the barrier properties of polyimide nanocomposite drastically. In general, for polymer films containing conventional clay type fillers, clay loading levels of up to 40%(wt/wt) are required to reduce the permeability of the clay filled structure. The observed increase in the barrier performance of the nanocomposite is attributed to the molecular level dispersion and specific geometry (thin plate) of the clay layers in the polymer entity. Those facts result in a large interfacial area between the clay and the polymer matrix and lead to excellent barrier properties.

Error Analysis

I. Uniformity of the nanocomposite films

The uniformity of the test films introduced the most variation in this study. Each sample of film was prepared by an individual batch procedure. Even for the pure polyimide films, variations may occur when using polymer solutions from a different condensation polymerization series. In addition, when preparing polyimide-clay composites, variation in stirring efficiencies in the reaction vials may result in different aspect ratios (L / W) for the clay particles. Finally, each film was cast on individual glass plates. Differences in surface properties of the respective glass plates may result in variation of film structure which may effect the orientation of the films and tortuosity of the permeant diffusing through.

It is assumed that the diffusion coefficient would be most impacted by a lack of uniformity of the polyimide films.

II. Thickness variance of the films

All of the variables described above can contribute to differences in the individual film samples in terms of the film thickness. The following is an example of thickness variation for a 2.5 v/v% Polyimide-clay film, at an ethyl acetate vapor activity of $a_v = 0.68$. (Table 15)

Table 15. Thickness distribution of the test film (2.5v% polyimide-clay) for the sorption of ethyl acetate at $a_v = 0.68$ and T = 23°C.

	1	2	3	4	5	6	μ	σ
Thickness (mil)	0.75	0.80	0.85	1.05	0.90	0.85		
	7	8	9	10	11	12	**0.908**	**0.090**
Thickness (mil)	1.00	0.90	1.00	1.00	0.90	0.90		

The variation of the thickness can account for the variation observed for the diffusion coefficient values.

III. Concentration variance of the permeant

The concentration of the ethyl acetate vapor in the hangdown tube can effect the partial pressure of the sorbate, which can directly impact the sorption value used in calculating the diffusion coefficient, especially in the very beginning of the experiment. The volume of the hangdown tube (i.e. 500cc) is significant. At the start of the sorption experiment, the volume is void of permeant vapor. While in an ideal test simulation, the volume in the electrobalance hangdown tube should instantaneously be filled with the desired vapor concentration at the time of experiment initiation, the physical design of the apparatus do not make this possible.

At an operating flow rate of 15 cm^3/min, the time required for the vapor concentration in the hangdown tube to approach 95% of the desired level would be approximately 2 hours. Figure 27 shows the plot of the ethyl acetate vapor concentration as a function of time. Compared to the time values to equilibrium (Table 4, Page 59), the time to reach the desired vapor concentration level would likely be minimal. Thus, the time required for displacement of the electrobalance hangdown tube volume by the penetrant vapor stream has introduced a small fraction of error into the diffusion coefficient values.

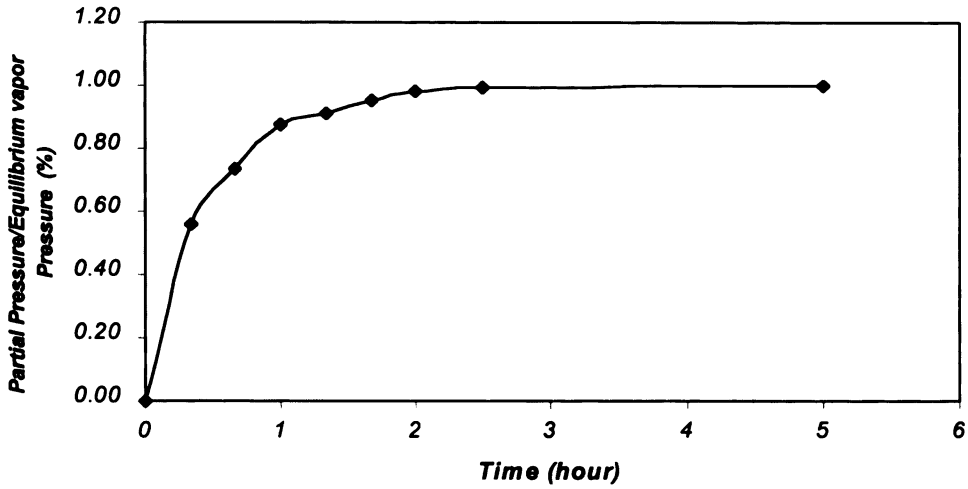

Figure 27 Equilibrium vapor pressure in the lower portion of the electrobalance hangdown tube as a function of time.

IV. Temperature variance of testing system

Temperature changes would effect the speed of the molecular movement and would effect the equilibrium solubility, as well as result in a change in the ratio of diffusivity. This is therefore an important variable in determining the diffusion coefficient. In the present study, the temperature of the test system was at ambient temperature (23 ± 1 °C) and would fluctuate with building temperature fluctuation. A typical plot of temperature versus time is presented in Figure 28. The solid line in Figure 28 is the vapor uptake profiles.

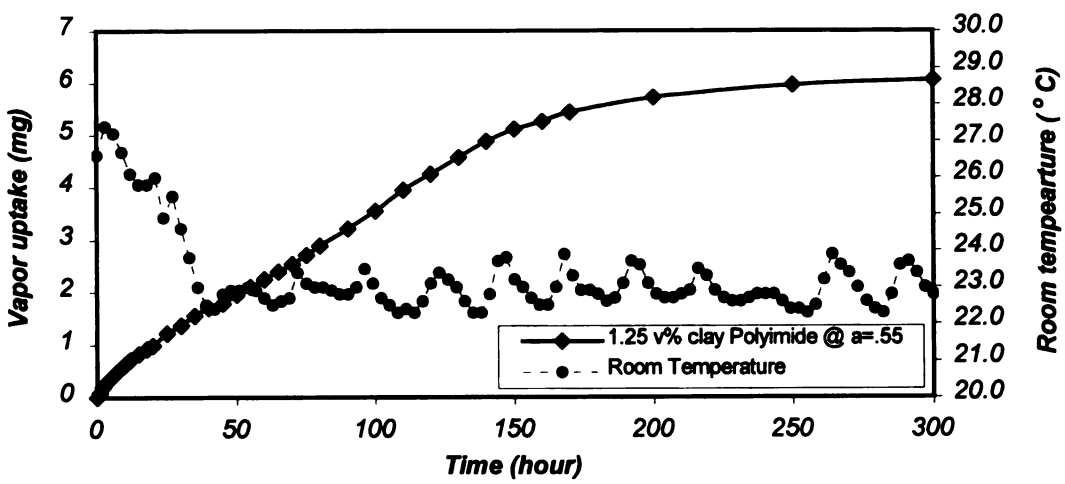

Figure 28 1.25v% Polyimide-clay composite sorption profile under alternating system temperature.

As shown, the highest temperature was 27.2 °C, the lowest temperature was 22.1°C, with a mean temperature at 23.23 ± 1.04 °C.

V. Non-Fickian sorption behavior

During the sorption of ethyl acetate by the non-clay polyimide films and clay-loading films, the experimental curve was found to deviate from the theoretical data. The higher the vapor activity, the greater the departure from the theoretical data and the higher the residual error. These findings can be explained by sorption induced swelling of the polymer matrix, resulting in the sorbate/polymer system exhibiting non-Fickian behavior. Table 16 summarizes the residual error, over the whole vapor activity range. The dramatic changes observed at the vapor activity values greater than 0.3 are evident.

Table 16 Residual errors by the Gauss-Newton curve fitting method as a function ethyl acetate vapor activity.

Vapor Activity	Residual Error By Gauss-Newton method	Diffusion Coefficient By Gauss-Newton method	Diffusion Coefficient By Least Squares method
0.15	0.044	0.347×10^{-16}	0.401×10^{-16}
0.21	0.045	0.460×10^{-16}	0.537×10^{-16}
0.27	0.045	0.479×10^{-16}	0.608×10^{-16}
0.44	0.084	0.884×10^{-16}	1.290×10^{-16}
0.55	0.085	1.380×10^{-16}	1.725×10^{-16}
0.68	0.090	2.780×10^{-16}	3.290×10^{-16}

Summary and Conclusion

The sorption of ethyl acetate vapor by polyimide-clay nanocomposite films was determined with the Cahn 2000 electrobalance, using a gravimetric technique and recording the weight gain by the polymer sample as a function time and vapor activity. The clay loading content and the organic vapor activity are the two major factors affecting the sorption and diffusion properties of polyimide-clay nanocomposites. For this nanocomposite film, montmorillonite is dispersed homogeneously within the polyimide matrix and oriented parallel to the film surface.

No significant change was found in the solubility values at equilibrium between the non-clay films and clay loading films, over the range of testing vapor activity levels studied. The equilibrium solubility values of polyimide-clay nanocomposite films could be accurately estimated by the total value of the independent unfilled polymer and the clay powder itself. The results of sorption studies showed that the polymer matrix and clay filler have similar organic vapor absorption properties, and the clay has neither a synergetic or antagonistic effect on the solubility of organic vapor in the polyimide matrix.

Comparison of the solubility coefficient values obtained for the non-clay films and clay loading films showed the values to be reasonably consistent, over the range of vapor activity levels studies. Because of the imperceptible changes in equilibrium solubility between the polyimide-clay hybrid and the simple polyimide matrix, over the

entire range of activity levels studied, the organic vapor solubility coefficient values were not effected by the presence of the clay inclusion. According to the dual mode sorption model, the solubility coefficient value would appear to be a constant value, represented by Henry's law constant, k_D, at medium and high vapor activity. Compared with the water sorption data, the small values of k_D and the large values of C'_H (Langmuir capacity constant) are characteristic of ethyl acetate vapor sorption in the polyimide films.

The exponential relationship found between the average diffusion coefficient and the vapor activity for the test systems evaluated can be explained by 'plasticizing' of the polymer matrix by the organic vapor, thus enhancing polymer chain segmental mobility as penetrant molecules are inserted between polymer segments, and resulting in an increasing in more free volume available for penetrant diffusion. The free-volume theory well described the molecular origin of the exponential dependence of the diffusivity on penetrant concentration and polymer free volume. The observed increase in the diffusion coefficient, with increased solute content in the polymer, should not lead to a value larger than that of the solute self-diffusion coefficient. In this study, the diffusion coefficient increase around tenfold, over a vapor activity range from the vacuum state to saturated state. In the case of the polyimide-clay nanocomposite of 1.25 v/v% clay loading, the diffusion coefficients increase about six-fold, when vapor activity increased from 0.3 to 0.7.

Such dependence found between the diffusion coefficient and the clay loading content of the nanocomposites can be the result of the effect of the aspect ratio and

tortuosity. Due to the specific structure, it is assumed that montmorillonite was dispersed homogeneously and disposed parallel to the film structure. As a result, the polyimide-clay nanocomposite had excellent vapor barrier properties. Only a small volume fraction of clay will result in a significant decrease in the diffusion coefficient. The diffusion coefficient of a 5.0 v/v% clay/polyimide film at vapor activity $a_v = 0.68$ is only one third of the diffusion coefficient value of the comparable non-clay polyimide film. The greater the level of clay loading, the lower the effectiveness of penetrant diffusivity, at the same penetrant concentration. This result is well explained by an increase in the tortuosity factor. The effective clay aspect ratio of approximately 100 from the ethyl acetate sorption in the present studies fell within the range reported in the literature. The observed increase in the barrier performance of the nanocomposite is attributed to the molecular level dispersion and specific geometry (thin plate) of the clay layers in the polymer entity. Those facts result in a large interfacial area between the clay and the polymer matrix and lead to excellent barrier properties.

Thus, the clay loading content, sorbate concentration and specific geometry of the clay layers in the polymer matrix would provide the polyimide-clay nanocomposites with unique properties for application in the packaging area.

Recommendation and Proposed Future Studies

Base on the results of this study, a number of recommendations for future research can be suggested. The following proposed studies might lead to a better understanding of the mass transfer of low molecular weight penetrants through the polyimide nanocomposites.

1. Due to the time constriction, this study only conducted one run for the sorption experiments involving the polyimide-clay nanocomposite films. It is proposed to duplicate the sorption experiments for the clay-loading polyimide films (1.25 v/v% ~ 5.0 v/v%) at vapor activity a_v = 0.21, 0.27, 0.34, 0.44, 0.55, 0.68.

2. Ethyl acetate was picked as the sorbate in this study because of its presence in many food flavor profiles. A similar study comparing the solubility and diffusion coefficient values should be made using a series of sorbates of varying molecular mass.

3. The current studies was conducted at RH = 0. It can be proposed that a similar investigation be conducted as a function of relative humidity (i.e. 50%, 95%) to investigate how the moisture affects the sorption mechanism for organic penetrants..

4. In this study, all sorption measurements were conducted at ambient temperature. It is proposed that additional experiments be conducted over a range of temperatures, to investigate:

   i) whether the temperature dependence of the solubility, and diffusion coefficient values can be described by the Arrhenius equation,

   ii) whether the solubility, and diffusion values agree as a function of temperature.

5. Sorption by non-clay and clay loading-polyimide films should be determined at lower ethyl acetate activity levels (i.e. a_v = 0.01, 0.02, 0.05, 0.1) where feasible, to understand how well the experiment data fits the dual-mode sorption model.

.

APPENDICES

Appendix A

Vapor-Liquid Equilibria for pure substances (VLPT)*

Ethyl acetate (Ethanoic acid ethyl ester, Ethyl ethanoate): $C_4 H_8 O_2$

141-78-6 M = 88.1063

Coefficients: $a_1 = 21.1891$ $a_2 = 2838.03$ $a_3 = -56.5630$

T (°C)	*p* (mmHg)
-20	6.390
-15	9.149
-10	12.874
-8	14.629
-5	17.262
-4	18.681
0	24.359
2	27.462
4	30.893
6	34.679
8	38.848
10	43.432
12	48.463
14	53.973
16	59.998
18	66.576
20	73.745
21	77.564
22	81.546
23	**85.697**
24	90.022
25	94.527
30	119.950
40	187.850
60	417.980

* CRC Handbook of Thermophysical and Thermochemical Data. (David R. Lide & Henry V. Kehiaian)

Appendix B

Basica Program for Diffusion Coefficient by "Consistency for Continuos Flow" Method[♣]

```
10    REM sorption continuous flow experiment
20    DIM F980), T(80), x(80), DF(80)
30    REM   time -- minute, D -- m^2/sec
40    INPUT "Enter the thickness of the film (MIL) -- ", LL
50    INPUT "Enter the steady state sorption value (mg) -- ", FI
60    NUM = 0 : N1 = 1: N2=1
70    DF(NUM+1) = F(NUM+1)/FI
80    READ T(NUM1), F(NUM+1)
90    DF(NUM+1) = F(NUM+1)/FI
100   IF T(NUM+1) = 99.99 THEN 140
110   PRINT T(NUM+1), F(NUM+1)
120   NUM = NUM+1
130   GOTO 80
140   GUESS = 10                                    'SET INITIAL GUESS

150   REM NEW-RAPHSON METHOD
160   FOR I=1 TO NUM
170   IF DF(I) < 0.05 AND DF(I+1) >= 0.05 THEN N1=I+1
180   IF DF(I) < 0.95 AND DF(I+1) >= 0.95 THEN N2=I
190   NEXT I
200   FOR I = N1 TO N2
210       A = 0.44313 * DF(I)                       'SQRT(π)/4 = 0.44313
215       X = GUESS
220   FOR J= 1 TO 10
230   B = SQR(X)
235   C = EXP(-X)
240   H = (0.5/B - B) * C
250   X = X- ((B*C - A)/H)
260   IF X <0 THEN GUESS = SQR(GUESS) : GOTO 215
270   NEXT J
280   X(I) = 1/X
290   GUESS = X
300   NEXT I

305   REM LINEAR REGRESSION
310   ST = 0
320   SX = 0 : SXT = 0
330   STSQ = 0
```

[♣] Referenced by Burgess and Hernandez, 1998.

```
340   SXSQ = 0
350   NN = N2 - N1 + 1
360   FOR I = N1 TO N2
370       ST = ST + T(I)
380       SX = SX + X(I)
390       SXT = SXT + X(I) * T(I)
400       SXSQ = SXSQ + X(I) * X(I)
410       STSQ = STSQ + T(I) * T(I)
420   NEXT I
430   SLOPE = (ST * SX - NN * SXT)/(ST * ST - NN * STSQ)
440   DUM1 = (NN * SXT) - (SX * ST)
450   DUM2 = (NN * STSQ) - (ST * ST)
460   DUM3 = (NN * SXSQ) - (SX * SX)
470   DUM4 = SQR(DUM2 * DUM3)
480   R= DUM1/DUM4
490   LPRINT LL; "MIL, "; ' 1.25V% Clay/Polyimide Film at Ethyl Acetate Vapor"
500   LPRINT
510   LPRINT "Time   (min) ", "Weight gain", "   1/X", "Relative Percentage"
520   FOR I = 1 TO NUM
530   LPRINT T(I), F(I), X(I), DF(I)
540   NEXT I
550   LPRINT
555   LPRINT "STEADY STATE SOLUBILITY  "; FI; "mg"
560   LPRINT
570   DIFF = ((LL * 0.0000254)^2)/4/60 * SLOPE
580   LPRINT "DIFFUSION COEFFICIENT (m2/sec)  ="; DIFF
590   LPRINT
600   LPRINT "CORRELATION COEFFICIENT       =", R

610   REM CONSISTENCY
620   FI1 = FI / 4
630   I = 1
640   I = I + 1
650   IF DF(I) < 0.25 GOTO 640
660   T14 = T(I - 1) + (T(I) - T(I - 1)) / (F(I) - F(I - 1)) * (FI1 - F(I - 1))
670   I= I + 1
680   IF DF(I) < 0.5 GOTO 670
690   T12 = T(I - 1) + (T(I) - T(I - 1)) / (F(I) - F(I - 1)) *( FI1 * 2 - F(I - 1))
700   IF I = NUM THEN 730
710   I = I +1
720   IF DF(I) < 0.75 GOTO 700
730   T34 = T(I - 1) + (T(I) - T(I - 1)) / (F(I) - F(I - 1)) * (FI1 * 3 - F(I - 1))
740   LPRINT
750   LPRINT "T □"; T14, " T □"; T12, " T □"; T34
760   X14 = 1/(SLOPE*T14) : X12 = 1/(SLOPE*T12) : X34 = 1/(SLOPE*T34)
770   PRINT "X14 "; X14, " X12 "; X12, " X34 "; X34
```

```
780   LPRINT "K1 "; X34/X14, " K2 "; X12/X14
790   LPRINT
800   END

810   DATA
820   DATA
830   DATA 99.99,99.99
```

Bibliography

American Colloid Company web page, 1998. "American Colloid Company - industrial specialist". Web address "http://www.colloid.com/finechm.htm"

Bandosz, T. J., 1992. "Chemical and Structure Properties of Clay Minerals Modified by Inorganic and Organic Materials". *Clay Minerals*, **27**, 435.

Barr, C. D., 1997. "A Comparison of Solubility Coefficient Values Determined by Gravimetric and Isotatic Permeability Technologies.", *Master Thesis*, School of Packaging, Michigan State University.

Barrer, R. and Barrie, J., 1957. *Journal of Polymer Science*, **23**, 315.

Blumstein, A., 1965. "Polymerization of Adsorbed Monolayers. II. Thermal Degradation of the Inserted Polymer". *Journal of Polymer Science*, Part A. **3**, 2665

Blumstein, R., 1974. "Acrylonitrile in Macromolecules". *Apply. Polym. Symp.*, **25**, P 81. Chicago, August 1974.

Burgess, G. and Hernandez R. J., 1998. PKG 985 course pack.

Chen, Yan and Wang, Xinyu, 1997. (Institute Chemistry, Chinese Academy Science, Beijing, P. R. China). *Gaofenzi Xuebao*, **1**, 73-78(Chinese).

Coleman, M. R. and Koros, W. J., 1990. *J. Membrane Sci.*, **50**, 285.

Crank, J. and Park, G. S., 1951. *Trans. Faraday Soc.*, **45**, 240.

Crank J., 1975. "The Mathematics of Diffusion". Academic Press, New York, NY.

Dupont Corporate home page, 1999. "Dupont Packaging". Web address "http://www.dupont.com/packaging/"

Dupont Polybon (polyimide), 1998. "DuPont Aerospace Enterprise". Web address "http://www.dupont.com/corp/markets/aerospace/"

Flory P. J., 1953. "Principles of Polymer Chemistry".

Fukushima, Y. and Inagaki, S., 1987. "Synthesis of an Intercalated Compound of Montmorillonite and 6-Polyamide". *J. Inclusion Phenom.*, **5**, 473

Fukushima, Y., Okada, A. and Kawasumi, M., 1988. "Swelling Behavior of montmorillonite by Poly-6-amide". *Clay Miner.* **v. 23,** 27

Gavara, R. and R. J. Hernandez, 1993. "Consistency Test for Continuos Flow Permeability Experimental Data". *Journal of Polymer Film and Sheeting*, **9**: 126

Ghosh, M. K., 1996. "Polyimides Fundamental and Applications".

Gilman, J. W., Kashiwagi, T., and Lichtenhan, J. D., 1997. Web address "http://flame.cfr.nist.gov/bfrlpubs/fire97/art015.html"

Greenland, D. J., 1963. "Adsorption of Polyvinyl Alcohol by Montmorillonite". *Journal of Colloid Science,* **18**, 647.

Gu, Jiajin, 1997. "The Barrier Characteristics of Clay/Polyimide Nanocomposites", *Master Thesis*, School of Packaging, Michigan State University.

Fukushima, Y., and Inagaki, S., 1987. "Synthesis of an Intercalated compound of Montomorilonite and 6-Polyamide". *J. Inclusion Phenom.*, **5**, 473,

Hernandez, R. J., Giacin, J. R., and Baner, A. L., 1986. "The Evaluation of the Aroma Barrier Properties of Polymer Films". *Journal of Plastic Film and Sheeting*, **2**(3); 187-211

Hernandez, R. J., Giacin, J. R., and Grulk, E. A., 1992 "The Sorption of Water Vapor by an Amorphous Polyamide". *J. Membrane Sci.*, **65**: 187-199.

Hernandez, R. J., 1994. "Effect of Water Vapor on the transport properties of oxygen through polyamide packaging materials". *J. of Food Engineering* **22**: 495-507.

Hernandez, R. J. 1998. Personal communication. Nov. 23, 1998.

Hirschfelder, J. O., Curtis, C. F., and Bird, R. B., 1954. *Molecular Theory of Gases and Liquids*, New York, P294.

Hopfenberg H. B. and Stannett V., 1973. "Physics of Glassy Polymers" (Ed. By R. N. Haward) Applied Science Publishers, Banking. **Chapter 9**, 504.

Kato, C., Kuroda, K., and Misawa, M., 1979. "Preparation of Montmorillonite-nylon Complexes and Their Thermal Properties". *Clays Clay Miner.*, v. **27**, 129 - 136

Koros, W. J., Fleming, G., K., Jordan, S. M., Kim, T. H., and Hoehn, H. H., 1988. *Prog. Polymer* Sci., **13**, 339.

Kim, Y.; Lee, W. K., Cho, W. J., Ha, C. S., Ree, M., and Chang, T., 1997. (Department of Polymer Science and Engineering, Pusan National University, Pusan, 609-735 S. Korea). "Morphology of organic-inorganic hybrid composites in thin films as multi-chip packaging material." *Polymer Int.* **43(2),** 129-136 (ENG).

Kim, T. H., Koros, W. J., Husk, G. R., and O'Brien, K. C., 1988. *J. Membrane Sci.*, **37**, 45.

Lagaly, G., and Beneke, K., 1975. "Intercalation and Exchange Reactions of Clay Minerals and Non-clay Layer Compounds". *American Mineralogist*, **60**, 650 - 658.

Lan, T., 1994. "Polymer-Clay Nanocomposite", *Ph.D. dissertation*, Michigan State University.

Lan, T., and Pinnavaia T., 1994(a). "On the Nature of Polyimide-Clay Hybrid Composites", *Chemistry of Materials, American Chemical Society*, **Vol. 6, (5),** 573-575.

Li, Qiang and Zhao, Zhudi, 1997 (State Key Lab. Engineering Plastic, Institute Chemistry, Chinese Academy Science, Beijing, P. R. China). *Gaofenzi Xuebao* 1997, (**2**), 188-193 (Ch).

Mark, J. E., 1995. (Polymer Research Center, University Cincinnati) *Int. SAMPE Tech. Conf.* **27**, 539-548.

Meares, P., 1993. *European Polymer Journal*, **29**, 237.

Mehrotra, V., and Giannelis, E. P., 1990. "Polymer Based Molecular Composites", *MRS Symp. Proc.,* D. W. Schaefer J. E. Mark, Eds., MRS. Pittsburgh, 171.

Messersmith, P. B. and Giannelis, E. P., 1993. "Polymer-layered silicate nanocomposites". *Chem. Mater.* **5**, 1064 - 1066.

Messersmith, P. B. and Giannelis, E. P., 1995. "Synthesis and Barrier Properties of Poly (ε - caprolactone) - Layered Silicate Nanocomposites". *Journal of Polymer Science*, **33**(7), 1047-1057.

Michaels, A., Vieth, W., and Barrie, J., 1963. *Journal of Applied physics,* **34 (1),** 1 & 13.

Myunghoon Lee, 1994. "Sorption of Organic Penetrants by Amorphous Polyamide" *Master Thesis*, School of Packaging, Michigan State University.

Nakamura, A., Ninomiya, K., Tamura, Y., 1989. *Kagaku Kogaku*, **53**, 646.

Nanocor, Inc. web page, 1997. "Nanocomposites". Web address "http://www.nanocor.com/ "

Neogi, P., 1996. "Diffusion in Polymers"

Nielsen, L., 1967. *Journal of Macromolecular Science Chemistry*, **A1** (5), 929

Okada, A., Kawasumi, M., Usuki, A., Kojima, Y., Kurauchi, T., and Kamigaito, O., 1990. *Mat. Res. Soc. Symp. Proc.* **171**, 45-50.

Okamoto K., Tamihara N., Watanabe H., Tanaka K., Kita H., Nakamura A., Kusuki Y., and Nakagana K., 1992. " Sorption and Diffusion of Water Vapor in Polyimide Films". *Journal of Polymer Science: Polymer Physics Edition* **30**: 1223.

Okamoto K., 1996. "10 Sorption and Diffusion of Water Vapor in Polyimide Film", *Polyimides, Fundamentals and Applications.*

Pace, R. J., and Datyner, A., 1980. "Model of Sorption of Simple Molecules in Polymers" *Journal of Polymer Science: Polymer Physics Edition*, **Vol. 18**, 1103 - 1124.

Paul D. R., and Yampol'skii, Y. P., 1994. *Polymeric gas separation membranes.*

Perrin, L., Nguyen Q. T., Clement R., and Neel J., 1996. "Sorption and Diffusion of Solvent Vapors in PVA Membranes of Different Crystallinity Degrees" *Polymer International*, Vol. **39**, No, 3, 251 - 260.

Pinnavaia, 1997. Web address "http://slater.cem.msu.edu/~pinnweb/nanocomposites.html"

Ruiz-Hitzky, E., 1993. "Conducing Polymers Intercalated in Layered Solids". *Adv. Mater.* **2(1)**, 545 - 547.

Taylor, John R., and Hernandaz, R. J., 1982. "An Introduction of Error Analysis", University Science Books.

Tohoh, M., 1992. European Patent, 0479031

Toshiyuki Momma, 1997. Corrosion Research Center, University of Minnesota. Web Page: "http://www.cems.umn.edu/crc/NanoComposite_Momma.html"

Triton Systems Inc., 1997. Web Page:
http://www.aro.ncren.net/arowash/rt/a_1page81.html"

Usuki, A., Okamoto K., Okada, A., and Kurauchi T., 1989. U.S. Patent 4,889,885.

Usuki, A., Koiwai, A., Kojima, Y., and Okada, A., 1995. "Interaction of Nylon 6-clay Surface and Mechanical Properties of Nylon 6-Clay Hybrid." *J. of Applied Polymer Sci.*, **v.5**, No. 1, 119-123

Usuki, A., Okamoto, K., Okada, A., and Kurauchi, T., 1995(a). "Synthesis and Properties of Acrylic Resin-Clay Hybrid". *Japanese Journal of Polymer Science and Technology*, **v.52**, No. 11, 727 - 733

Vaia, R. A., Ishii, H., and Giannelis, E. P., 1993. "Synthesis and Properties of two-dimensional nanostructures by direct intercalation of Polymer melts in layered silicates". *Chem. Mater.*, **v. 5**, 1694 - 1996.

Vaia, Richard A.; Sauer, Bryan B.; Tse, Oliver K.; Giannelis, and Emmanuel P., 1997. (Department of Materials Science and Engineering, Cornell University, Ithaca, NY 14853 USA). *J. Polymer Science, Part B: Polymer Physics* **35**(1), 59-67 (Eng), Wiley.

Vieth, W. R., Howell J. M., and Hsieh, J. H., 1976. "Dual Sorption Theory" *Journal Membrane Sci.*, **1**, 177.

Vieth, W., Tam, P. and Michaels, A., 1966. *Journal of Colloid and Interface Science*, **22**, 360-370.

Wensa, 1999. "Polymer-Clay Nanocomposites"
Web Page:"http://www.geocities.com/Tokyo/Garden/2116/nano_polymer.htm"

Yano, K., Usuki, A., Okada, A., Kurauchi, T., and Kamigaito, O., 1991. "Synthesis and Properties of Polyimide-Clay Hybrid". *Polymer Preprint*, **32(1)**, 65.

Yano, K., Usuki, A., Okada, A., Kurauchi, T., and Kamigaito, O., 1993. "Synthesis and Properties of Polyimide-Clay Hybrid". *J. Polymer Sci.: Part A: Polymer Chemistry*, **v. 31**, 2493.

Yano, K., Usuki, A., and Okada, A., 1997. "Synthesis and Properties of Polyimide-Clay Hybrid Films". *J. Polymer Science: Part A: Polymer Chemistry,* **35(11)**, 2289-2294.

Ziegel, K. D., Frensdorff, H. K., and Blair, D. E., 1969. "Measurement of Hydrogen Isotope Transport in PVC Films by Permeation Rate Method". *Journal of Polymer Science*, Part A-2, 7: 809